



TALLINN UNIVERSITY OF TECHNOLOGY
SCHOOL OF ENGINEERING
Department of Electrical Power Engineering and Mechatronics

**USE OF MACHINE LEARNING AND
HYPER SPECTRAL IMAGING FOR MATERIAL
CLASSIFICATION**

**MASINÕPPE JA HÜPERSPEKTRAAL PILDITEHNIKA
KASUTAMINE MATERJALIDE KLASSIFITSEERIMISEKS**

MASTER THESIS

Student: Ramin Madani

Student code: 184674MAHM

Supervisor: Dr. Mart Tamre

Co-supervisor: Dr. Aleksei Tepljakov

Tallinn 2020

(On the reverse side of title page)

AUTHOR'S DECLARATION

Hereby I declare, that I have written this thesis independently.

No academic degree has been applied for based on this material. All works, major viewpoints and data of the other authors used in this thesis have been referenced.

"18" May 2022

Author: Ramin Madani

/signature /

Thesis is in accordance with terms and requirements

"18" May 2022

Supervisor: Mart Tamre

/signature/

"18" May 2022

Co-supervisor: Aleksei Tepljakov

/signature/

Accepted for defence

".....".....20... .

Chairman of theses defence commission:

/name and signature/

Non-exclusive licence for reproduction and publication of a graduation thesis¹

I, Ramin Madani

1. grant Tallinn University of Technology free licence (non-exclusive licence) for my thesis Use of Machine Learning and Hyperspectral Imaging for Material Classification,

supervised by Dr. Mart Tamre, Dr. Aleksei Tepljakov

1.1 to be reproduced for the purposes of preservation and electronic publication of the graduation thesis, incl. to be entered in the digital collection of the library of Tallinn University of Technology until expiry of the term of copyright;

1.2 to be published via the web of Tallinn University of Technology, incl. to be entered in the digital collection of the library of Tallinn University of Technology until expiry of the term of copyright.

2. I am aware that the author also retains the rights specified in clause 1 of the non-exclusive licence.

3. I confirm that granting the non-exclusive licence does not infringe other persons' intellectual property rights, the rights arising from the Personal Data Protection Act or rights arising from other legislation.

_____ (date)

¹ *The non-exclusive licence is not valid during the validity of access restriction indicated in the student's application for restriction on access to the graduation thesis that has been signed by the school's dean, except in case of the university's right to reproduce the thesis for preservation purposes only. If a graduation thesis is based on the joint creative activity of two or more persons and the co-author(s) has/have not granted, by the set deadline, the student defending his/her graduation thesis consent to reproduce and publish the graduation thesis in compliance with clauses 1.1 and 1.2 of the non-exclusive licence, the non-exclusive license shall not be valid for the period.*

Department of Electrical Power Engineering and Mechatronics

THESIS TASK

Student: Ramin Madani, 184674MAHM

Study programme, MAHM 02/18 - Mechatronic

main speciality: Mechatronics

Supervisor(s): Dr. Mart Tamre, 5120982, Dr. Aleksei Tepljakov, 6202116

Consultants: None

Thesis topic:

(in English) Use of Machine Learning and Hyperspectral Imaging for Material Classification

(in Estonian) Masinõppe ja hüperspektraal pilditehnika kasutamine materjalide klassifitseerimiseks

Thesis main objectives:

1. Investigate the application of machine learning and spectral processing methods for the task of material classification with hyperspectral images as the ground data
2. Apply or propose ideas methods for performance optimization for specific applications
3. Develop a GUI software tool for qualitative and quantitative analysis of hyperspectral images

Thesis tasks and time schedule:

No	Task description	Deadline
1.	Understanding the problem and initial analysis	05.09.2021
2.	Finalizing the code for the MATLAB GUI application	02.10.2021
3.	Reviewing the relevant literature	15.10.2021
4.	Preparation of the initial code for solving the problem	25.10.2021
5.	Further study of the topics involved in the field	10.12.2021
6.	Forming the idea about the methods and developing the code	20.01.2022
7.	Preparing thesis sketch	25.02.2022
8.	Finalizing the development of the code for models	27.03.2022
9.	Writing the thesis work	10.05.2022

Language: English **Deadline for submission of thesis:** "18" May 2022.a

Student: Ramin Madani "18" May 2022a

/signature/

Supervisor: Dr. Mart Tamre "18" May 2022a

/signature/

Co-supervisor: Dr. Aleksei Tepljakov "18" May 2022a

/signature/

Head of study programme: Dr. Anton Rassölkin "....."2022a

/signature/

Terms of thesis closed defence and/or restricted access conditions to be formulated on the reverse side

TABLE OF CONTENTS

PREFACE	13
List of abbreviations.....	14
1. INTRODUCTION.....	15
1.1. Problem Statement.....	16
1.2. Thesis structure	17
1.3. Research Questions	18
2. LITERATURE REVIEW.....	19
2.1. Hyperspectral imaging and image processing	20
2.1.1. Introduction.....	20
2.1.2. Hardware (camera)	22
2.1.3. Illumination	23
2.1.4. Setup and the scene	24
2.1.5. Structure of the HS image files	25
2.1.6. HS Image preprocessing	25
2.1.7. History and some applications of HSI	25
2.2. Material classification for HSI with the use of ML and SM	26
2.2.1. Feature selection.....	26
2.2.2. The models.....	27
2.2.3. Evaluation	27
2.3. Software for HS image analysis and classification	29
2.4. Potential areas of focus (existing gaps)	30
3. MATERIAL CLASSIFICATION	31
3.1. Getting a general picture of the problem	31
3.1.1. The data points.....	31
3.1.2. The patterns in the skin spectral signature	32
3.2. Imaging	33
3.2.1. Imaging parameters	33
3.2.2. Selected imaging parameters.....	36
3.2.3. Camera calibration	37
3.2.4. The setup.....	37
3.2.5. The summary of the process.....	38
3.3. Dataset.....	38
3.3.1. Number of training instances	38
3.3.2. Class balance.....	38
3.3.3. Variety.....	39
3.4. Preprocessing	39

3.4.1. Image calibration	39
3.4.2. Imputation, numerical encoding	39
3.4.3. Filters	40
3.4.4. Outliers.....	41
3.4.5. Normalization	41
3.4.6. Selected preprocessing operations.....	42
3.4.7. Summary of the preprocessing operations	43
3.5. Selecting the features	43
3.5.1. The influence of feature selection	43
3.5.2. Different choices	44
3.5.3. Local extrema	44
3.5.4. Using variances.....	45
3.5.5. Summary of the feature selection operation.....	46
3.6. Selecting the models.....	47
3.7. Applying the models	48
3.7.1. Method 1: Spectral Matching (SM) using Spectral Angle Mapper (SAM)	49
3.7.2. Method 2: SM using Euclidean distance	51
3.7.3. Method 3: SM using a mixture of distance measures.....	52
3.7.4. Method 4: SM using a mixture of feature types and distance measures	54
3.7.5. Method 5: K-Nearest Neighbors (kNN)	56
3.7.6. Method 6: Artificial Neural Network (ANN)	57
3.8. Results of the evaluation	60
3.9. Summary of the results.....	61
4. THE SOFTWARE	63
4.1. The interface	63
4.1.1. Image display and spectral information	63
4.1.2. Image histograms	65
4.1.3. False RGB image	65
4.1.4. Data handling	68
4.2. Case study	68
4.2.1. Looking for the differences	69
4.2.2. Exposing the differences	70
4.2.3. Further processing.....	70
4.2.4. The usage flow to perform the task	71
4.2.5. Summary of the specifications	72
5. DISCUSSION AND FINAL REMARKS	73
5.1. Methods performance	73
5.2. Software	74

5.3. Applications	74
5.4. Verifying that the initial goals are met.....	75
5.5. Future work.....	75
5.6. Schematic summary of the operations and data flow.....	76
6. SUMMARY	77
KOKKUVÕTE	78
REFERENCES.....	79
APPENDICES	85
APPENDIX 1 Specim IQ camera specifications	86
APPENDIX 2 Workflow of Specim IQ for imaging.....	87
APPENDIX 3 ENVI standard parameters for HS images.....	88
APPENDIX 4 Wavelength-Band number mapping of Specim IQ.....	90
APPENDIX 5 Graphical material related to Chapter 2.....	91
APPENDIX 6 Graphical material related to Chapter 3.....	93
APPENDIX 7 The Code	95
APPENDIX 8 The Paper.....	96

TABLE OF FIGURES

Figure 2.1 Areas involved in this work, by indication of the connection to our research questions.....	19
Figure 2.2 The electromagnetic spectrum and the range of the spectrum that is usually captured in different HSI applications [6].....	20
Figure 2.3 Spectral and spatial information stored in a hyperspectral image (right), and the spectral signature curve derived for one pixel of the image (left) [7]	21
Figure 2.4 Spectral curves recorded in RGB and hyperspectral cameras [8]	22
Figure 2.5 Specim IQ camera [11], Semi-portable Resnon hyperspectral camera (middle), portable BaySpec hyperspectral camera (left) [12] and [13]	22
Figure 2.6 Spectra of halogen light from 350 nm to 750 nm wavelength [18].....	24
Figure 2.7 Image segmentation using HS images for plum fruit quality assurance [29]	26
Figure 2.8 Confusion matrix together with evaluation measures derived from it, for a classification problem with two classes "Positive" and "Negative"	28
Figure 3.1 The original image upon which the classification takes place	32
Figure 3.2 Spectral signature of different groups of data points	33
Figure 3.3 The spectral signature of human skin imaged under two different light sources	34
Figure 3.4 Two points of an object which are exposed to different light intensities[17]	35
Figure 3.5 An ideal camera/lighting positioning/orientation suggested for the Specim IQ camera by the manufacturer. X should be larger than 15 cm, α should be close to 45 degrees, and the distance of the camera's lenses to the object should not be less than 15 centimeters. [15].....	35
Figure 3.6 The imaging setup used in natural light	37
Figure 3.7 Summary of the steps involved in imaging.....	38
Figure 3.8 Spectral signature before applying Savitzky-Golay (left), and after applying it (right)	40
Figure 3.9 Spectral signature before applying average filter (left), and after applying it (right).....	40
Figure 3.10 Two kinds of abnormalities on human skin and on fruit skin resulting in outlier points.....	41
Figure 3.11 Spectral signatures of all the selected skin pixels as training/reference data	42
Figure 3.12 Summary of the steps involved in the preprocessing	43
Figure 3.13 Data points of two classes in feature space after feature reduction.....	44

Figure 3.14 The local minima and maxima of the spectral signature of skin pixel.	45
Figure 3.15 Variance between the classes and inside each class in selected dataset ..	46
Figure 3.16 Summary of the steps involved in feature selection.....	47
Figure 3.17 Categorization of the methods based on the general mechanism	48
Figure 3.18 Schematic view of methods in feature space. Method 1 (a), method 2 (b)	49
Figure 3.19 Points classified as skin in method 1	50
Figure 3.20 Points classified as skin in method 2	52
Figure 3.21 Schematic view of the third method's feature space (features are reflectance values).....	53
Figure 3.22 Points classified as skin in method 3	53
Figure 3.23 Schematic view of the fourth method's feature space (features are reflectance values, left, and 1 st derivative of the reflectance values, right).....	54
Figure 3.24 The derivative of the spectral signature of three groups of points	55
Figure 3.25 Points classified as skin in method 4	55
Figure 3.26 Data points in the feature space of intensities in kNN, and the sample (target) [58].....	56
Figure 3.27 Points classified as skin in method 5 (kNN).....	57
Figure 3.28 Network configuration in MATLAB	58
Figure 3.29 Points classified as skin in method 6 (ANN).....	59
Figure 3.30 Confusion matrices of the classification methods 1 through 6.	60
Figure 3.31 The image results of skin classification laid out via the six methods.	62
Figure 4.1 "Display" tab of the interface. This tab is the active tab when the application starts.	64
Figure 4.2 Spatial intensity map (right) at a certain region marked on the image (left)	64
Figure 4.3 "Histogram" tab, including three types of histograms and their corresponding images.....	65
Figure 4.4 The true RGB image (a), and two false RGB images (b) and (c)	66
Figure 4.5 "False RGB 2" tab. Reflectance intensity histograms and RGB ratio pie chart of the three bands	68
Figure 4.6 The true RGB image (a), and the generated False RGB image where the annotated apples are clearly distinguishable (b). On the left, the corresponding wavelengths that are interpreted as R, G and B bands can be found.	69
Figure 4.7 The fingerprint of a pixel on "Apple 1" (left), and on "Apple 2" (right). The three arrows show at what wavelengths the largest differences exist between the two apples' fingerprints	70
Figure 4.8 Flow of the actions taken to detect the difference between the two apples	71

Figure 5.1 The four evaluation measures of the methods used	74
Figure 5.2 Schematic summary of the operations and data flow in the scope of this thesis work	76
Figure A1 Specim IQ camera	86
Figure A2 Detailed workflow of Specim IQ for the imaging procedure	87
Figure A3 Spectral signature of different materials [66]	91
Figure A4 Image sample and spectral signatures of skins of 28 imaging subjects [26]	91
Figure A5 Different scanning techniques used in hyperspectral cameras [67]	92
Figure A6 Three popular file structures of a hyperspectral image (BSQ, BIL, BIP) [68]	92
Figure A7 Imaging setup when the light source is incandescent light	93
Figure A8 Some skin samples collected in the dark room setup from different subjects and different parts of the body	93
Figure A9 The range of the angular distances of the skin points to the reference point	94

LIST OF TABLES

Table 3.1 Summary of imaging parameters used	36
Table 3.2 Summary of preprocessing steps that were taken	42
Table 3.3 Specifications of the kNN model (Method 5)	57
Table 3.4 Specifications of the trained neural network model (Method 6).....	58
Table 3.5 Summary of the specifications of the models.....	59
Table 3.6 The summary of the evaluation results of methods 1 through 6.....	61
Table 4.1 GUI application specifications	72
Table A1 Technical specifications of Specim IQ camera [64]	86
Table A2 ENVI parameter and its definition according to ENVI standard [65].....	88
Table A3 List of the bands and their corresponding wavelengths in Specim IQ.....	90

PREFACE

The opportunity to conduct research on the topic of data classification led me to focus my attention toward topics related to machine learning and computer vision. It allowed me to investigate applying machine learning methods on imaging data for the purpose of classification of materials, and on the side, development of a graphical software tool to make analysis and processing of the imaging data more facile for people with an interest in this topic. As a further contribution, a paper was compiled and presented on the topic of the MATLAB graphical interface development for the analysis of hyperspectral images in co-operation with the supervisor and co-supervisor of this thesis work.

The general topic of material identification and usage of the hyperspectral imaging data for classification tasks has been introduced in the Department of Electrical Power Engineering and Mechatronics, School of Engineering at Tallinn University of Technology (Taltech) and related topics were offered by Professor Mart Tamre from the same department. Relevant practical work for this thesis is conducted at Tallinn University of Technology using the equipment and tools made available by the Laboratory of Mechatronics, and the relevant studies and consultations have majorly taken place at Taltech, Estonia, at the Royal Institute of Technology (KTH), Sweden, and individually by the author.

I would like to express my sincere gratitude to Dr. Mart Tamre and Dr. Aleksei Tepljakov, who kindly accepted to supervise and support me along this path. I have continuously benefited from the consultation, guidance and support that they have provided me with. I am also thankful for their patience and ongoing encouragement as it made taking this road easier than it could be. Their support spans not only along the period of my thesis work, but through the entire time of my study at Taltech.

Furthermore, I want to use this opportunity to thank all the professionals at Taltech's department of Electrical Power Engineering and Mechatronics, who made it possible for me to perform the tasks related to this work.

Keywords: classification, machine learning, GUI programming, hyperspectral imaging, robotics, mechatronics, computer vision, master thesis

List of abbreviations

Abbreviated Form	Expanded Form
AI	Artificial Intelligence
ANN	Artificial Neural Networks
BIL	Band-Interleaved by Line
BIP	Band-Interleaved by Pixel
BSQ	Band-Sequential
CNN	Convolutional Neural Networks
DL	Deep Learning
DNN	Deep Neural Networks
FC	Fully-connected
FF	Feed Forward
FN	False Negative
FP	False Positive
fRGB	False RGB (Red, Green, Blue)
GUI	Graphical User Interface
HS	Hyperspectral
HSI	Hyperspectral Imaging
kNN	k-Nearest Neighbors
LWIR	Long-wavelength Infrared
ML	Machine Learning
MV	Machine Vision
NIR	Near Infrared
NN	Neural Networks
OC	Object Classification
OS	Operating System
RAM	Random Access Memory
RGB	Red, Green, Blue
SAM	Spectral Angle Mapper
SL	Supervised Learning
SM	Spectral Matching
TN	True Negative
TP	True Positive
UV	Ultraviolet
WL	Wave Length or Wavelength

1. INTRODUCTION

Employing computers and computational algorithms to yield practical solutions in a vast amount of fields and applications has dramatically speeded up with the introduction of modern Artificial Intelligence (AI) fashions into the world of computer science. Machine Learning (ML), as a subset of artificial intelligence, has gained popularity in providing powerful efficient methods to perform tasks that used to be carried out by humans, and tasks that have never been possible to be performed by humans. In recent years, machine learning methods hand in hand with methods of computer vision have been utilized for operations such as localization of objects, recognition of human emotions, and classification of different materials based on their images [1]. In this regard, they have been successful to surpass human vision and perception systems in many areas such as the food industry, where robotic systems can categorize fruits with fascinating speeds, far faster than a human can deliver.

In parallel, the world of computer vision, digital imaging, and image processing have undergone numerous advancements. Conventional color imaging has been optimized in different ways, and techniques such as hyperspectral imaging have been made accessible to the public and to the researchers more widely. In color imaging, only a very limited amount of information from the reflecting light is captured by the cameras, and only a small portion of the light spectrum is registered (the visible light portion). In recent years, Hyperspectral Imaging (HSI) for ordinary usages has come to play and has flourished [2]. In hyperspectral imaging (HSI), along with spatial information, a significant amount of wavelength (spectral) information is registered (hundreds of times larger than conventional color imaging). Because of this broad range of spectral information, each material can be associated with a unique spectral signature that can be used for the identification of that material. This allows for the classification potential of hyperspectral imaging data to classify different materials.

Merging the two technologies in question, namely machine learning and hyperspectral imaging, allows for combination of the possibilities that each of these technologies provides. In other words, computational power together with artificial intelligence methods and the significant information by hyperspectral images gives humans the power to compile approaches for material classification more efficient than ever before.

There are many applications related to the different fields in engineering such as Mechatronics and Robotics that might be addressed if such combination is properly put to practical usage, but for this to come to effect, a number of items need to be

considered. First, according to the domain knowledge of every field and the possibilities of HSI in that respect, an approach needs to be developed for analyzing the current challenges in a field. Performing proper image acquisition, interpreting the imaging data, processing of the image, analyzing the possible ML solutions, and applying the computer classification methods on the imaging data are the next steps. It will be an advantage if such a system can be improved by proposing optimization approaches. Finally, to benefit general users of technology in that area, developing relevant software which may satisfy their needs can come into perspective.

In this thesis work, the focus has been on performing the mentioned tasks to address the challenge of the usage of computer learning and processing methods on HSI data for identification of different materials.

1.1. Problem Statement

With respect to what was pointed out, there are three major problems that have been focused on throughout this work.

The first is to develop a systemic approach to deploy classification models to problems related to the field of engineering (including Mechatronics) incorporating the spectral information of the hyperspectral images as the main data. The solution to this problem is in the scope of image data acquisition, analysis and preprocessing of the image data, selection of the features, creating a model for detection/classification, and testing of the results as the final step. The outcome of solving this problem will be working models for classification/identification of an entity in a specific domain.

As a second challenge, in parallel with the first problem, optimization is concerned, such that, where applicable, solutions for increasing the performance of the models in the specific domain of application should be proposed. To this end, methods of preprocessing and feature selection, and similarity measures need to be reviewed and also combination of such entities may be examined. The outcome will be an extension to an existing models, e.g. an engineered feature/similarity measure or a combination of features/similarity measures, whose usage increase the performance of the methods at the time of test.

The third problem that needs to be addressed is the development of a graphical user interface tool for the analysis and processing of hyperspectral images. It needs to provide the user with a self-explanatory interface where the minimum amount of time

should be needed for the process of learning to work with the software. Also, the needs of the users with mobile hyperspectral cameras need to be concerned. This problem falls in the scope writing GUI programs where the needs of the users, the existing software in the market, and integration of the code and the interface are important concerns. The outcome of solving this problem is a MATLAB GUI application for processing and analysis of HSI data.

The tools for solving the problems consist of hardware tools (hyperspectral camera, computation hardware, etc.), software tools (programming languages, GUI development environment, software toolboxes and libraries, engineering software, graphical software, etc.), and theoretical tools (mathematics, statistics, machine learning theory, machine vision, etc.). The data needed is the raw data coming from the acquiring of the hyperspectral images.

1.2. Thesis structure

This work has been compiled in 6 chapters. Chapter 1 is dedicated to the introduction of the work, which starts with a general introduction to the subject of the thesis, and continues by stating the problems, and talking about the needed tools and ends with the research questions.

In chapter 2, the reader gets familiar with the topics involved, and following that, background knowledge of HSI and a brief history and study of the applications is conducted. The same happens for the usage of machine learning in connection with HSI, and finally, the development of a software application for HSI is reviewed. The final section points out the potential areas of work in these areas. At the same time, the related literature is investigated.

Chapter 3 is dedicated to explaining the methodology of applying spectral matching and machine learning methods to hyperspectral data. In the beginning, hyperspectral image acquisition and its details are discussed and in the following parts,

In chapter 4, the development of the software for the analysis of hyperspectral images is discussed. Components of the software are explained and in the end, an example of the usage of the software is presented.

The discussions and final remarks about the work are put into perspective in chapter 5. In this chapter, the performance of the methods, the development of the application, and remarks about practical usage of the methods are put forward.

In chapter 6, a summary of the work is presented in English and Estonian, and following that, in the chapter titled "References" the list of references is provided.

"Appendices" chapter comes as the last chapter of the thesis including the reference tables, additional figures related to chapters 2 and 3, and additional references to the relevant paper and code. The address to the online code repository for the thesis-related code is made available, and in the final section, the information related to the conference paper that was compiled in regards to this topic is provided.

1.3. Research Questions

The three main research questions are as follows.

1. What are the tasks that need to be carried out to reach a model with the capability of binary classification to identify a specific material present in a hyperspectral image (with wavelength range of 400-1000)?, and how can a model be compiled and programmed for such tasks?
2. Is this possible to increase the performance of a material classification model in test with the evaluation criteria of accuracy and F1 score through modification of preprocessing operations, features or similarity measures?, and if possible, how can this be achieved?
3. What are the best arrangement of components and functions in a GUI software for qualitative and quantitative analysis and processing of hyperspectral images for users of portable hyperspectral cameras and based on the needs in science, academia and in practical usages?, and how can a GUI application with proper layout be developed to address this?

Keywords: classification, machine learning, GUI programming, hyperspectral imaging, robotics, mechatronics, computer vision, master thesis

2. LITERATURE REVIEW

Analysis and classification of materials using HSI data using machine learning and spectral processing approaches involve concepts and techniques which fall under the intersection of several different fields (Figure 2.1). Consequently, the review of the relevant literature encompasses the familiarity and overview of such various concepts and fields. Hence, in this chapter, the reader will be presented with a background on the involved topics and the literature will be reviewed alongside.

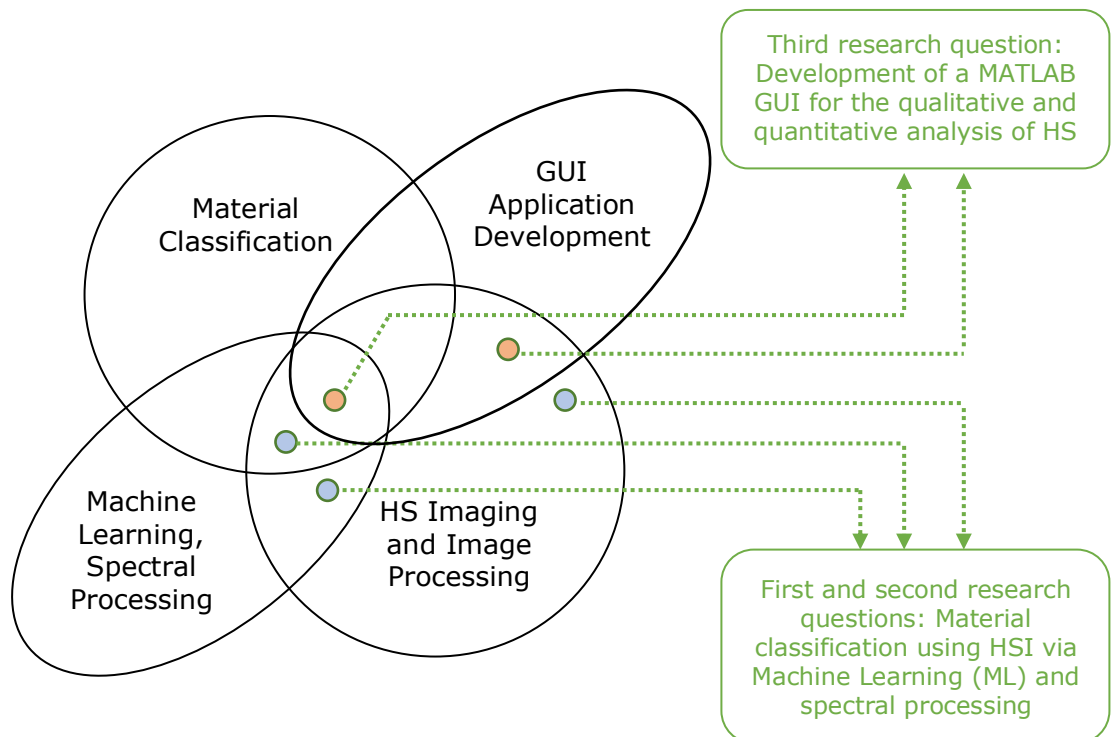


Figure 2.1 Areas involved in this work, by indication of the connection to our research questions

The main type of data that is in focus throughout this thesis work is the hyperspectral images data. So all the key concepts, techniques and related knowledge of Hyperspectral Imaging (HSI) are discussed in section 2.1. Continuing toward the fields of Machine Learning (ML) and the incorporation of computers in material classification, the second section (2.2) is dedicated to reviewing the previous works in these areas and how it has been linked with HSI. In section 2.3, appropriate software tools which might be developed in relation to HSI and the reason why there still is a drastic need in this area is reviewed. Finally, in section 2.4, it has been tried to identify what are the gaps in the current field of research and in relation to our research questions to clarify for the reader why this work has been compiled.

2.1. Hyperspectral imaging and image processing

The first section makes the user acquainted with important concepts of Hyperspectral Imaging (HSI) and Image processing, which are key for the continuation of the study.

2.1.1. Introduction

Hyperspectral Imaging (HSI) is an imaging technique that registers more wavelengths of light compared to the conventional color imaging or multispectral imaging methods, and has the possibility to cover wider ranges of the light spectrum. In other words, the registered range of the spectra in HSI may go beyond the scope of the visible range ($\approx 380\text{-}750\text{ nm}$) [3] [4] while the light striking each pixel is broken down into many different spectral bands (hundreds or thousands) in order to provide more comprehensive wavelength (WL) information on what is imaged [3].

The light that is captured by the camera in most HSI applications ranges from the ultraviolet (starting at $\sim 250\text{ nm}$) up to long-wave infrared (LWIR, $\sim 2500\text{ nm}$). Cameras usually record a subset of this range, like Visible to NIR (Near Infrared) which covers approximately $400\text{-}1300\text{ nm}$ (Figure 2.2) [5].

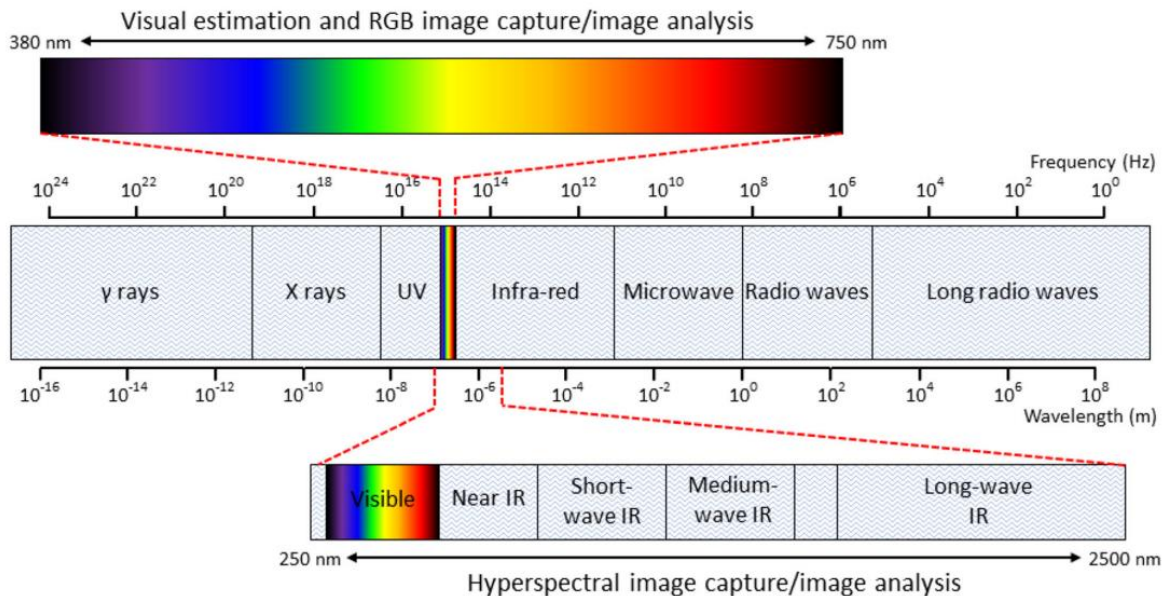


Figure 2.2 The electromagnetic spectrum and the range of the spectrum that is usually captured in different HSI applications [6]

The reflection of the light from any single point on a surface is decomposed and recorded by the camera in hundreds (or thousands) of wavelengths, and so for each pixel,

hundreds of reflectance values are registered. The set of all these values is known as the “spectral signature” or “fingerprint” of that specific pixel. As depicted in Figure 2.3, the spectral signature of a pixel (reflectance values) is possible to be graphed with respect to the wavelengths (or bands). Each point P on this graph can be represented by an ordered pair $(w_i, R^P(w_i))$, where w_i is the wavelength at band i in nanometers (nm), and $R^P(w_i)$ is the corresponding reflectance value in that wavelength of pixel P . In mathematical terms, when $R^P(i)$ is the reflectance (intensity) value of point P at band i , the spectral signature of a pixel (S_{Sig}^P) when the number of captures wavelengths (bands) is N_b , would be:

$$S_{Sig}^P = \{ (w_i, R^P(w_i)) \mid i \in \{1, 2, \dots, N_b\} \} \quad (2.1)$$

Or interchangeably,

$$S_{Sig}^P = \{ (i, R^P(i)) \mid i \in \{1, 2, \dots, N_b\} \} \quad (2.2)$$

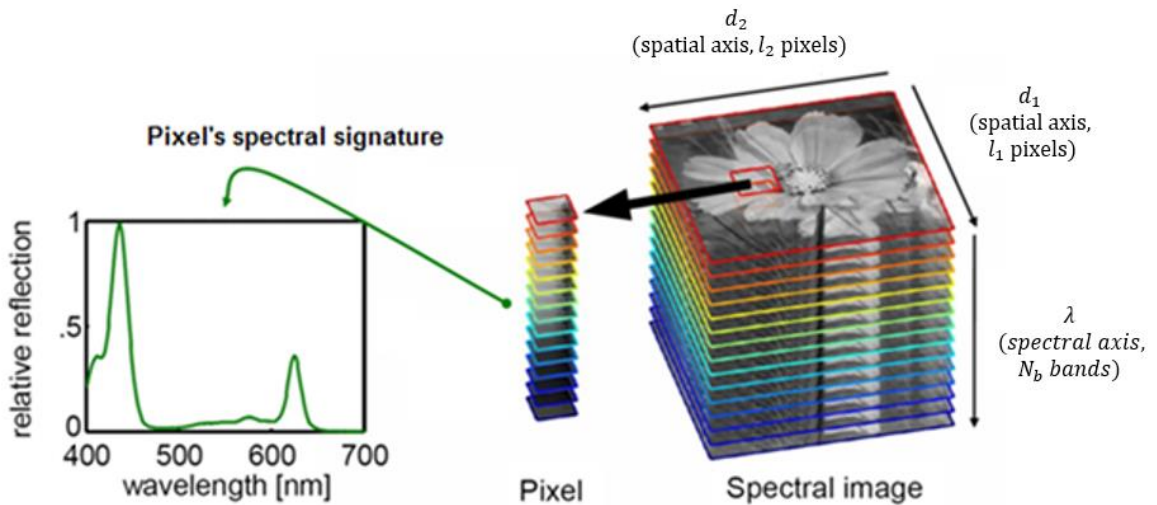


Figure 2.3 Spectral and spatial information stored in a hyperspectral image (right), and the spectral signature curve derived for one pixel of the image (left) [7]

The data that is captured by a conventional color camera is usually stored in three layers (bands), namely Red, Green, and Blue (RGB). Each of the bands may be presented by an l_1 pixel \times l_2 pixel grayscale image, or an l_1 by l_2 matrix whose elements represent light intensity (reflectance) values. For each of the pixels in an RGB image, we may graph the spectral signature as an intensity-WL diagram with three points (Figure 2.4, left).

Similarly, if N_b is the number of bands registered by the HS camera, and l_1 and l_2 are the spatial dimensions (height and width of the image), the image may be stored as a 3-dimensional $l_1 \times l_2 \times N_b$ matrix. In HSI terminology, this image matrix is known as the image data cube (data cube). The spectral signature of an HS image is hence formed with N_b points, from whose connection the spectral signature curve is shaped. More instances of the spectral signature of different materials are available in Figure A3 (appendices).

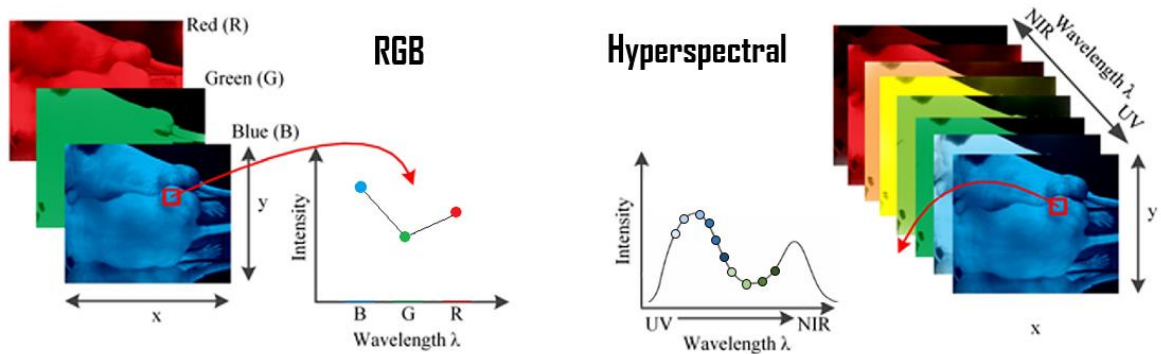


Figure 2.4 Spectral curves recorded in RGB and hyperspectral cameras [8]

2.1.2. Hardware (camera)

Portable HS cameras: With advances in hardware and optics design and miniaturization, as well as improvements in computational algorithms, the emergence and development of portable (mobile) hyperspectral cameras has started during the 2010s [9]. These developments led to the possibility of taking hyperspectral images with a normal-sized camera, compared to what has been possible previously [10]. Still, there are very few portable cameras available commercially, and still, their price is relatively high. Three of the models of mobile HS cameras are observable in Figure 2.5.



Figure 2.5 Specim IQ camera [11], Semi-portable Resonon hyperspectral camera (middle), portable BaySpec hyperspectral camera (left) [12] and [13]

Scanning technique: The four main imaging techniques used in HSI are illustrated in Figure A5 (appendices). The scanning technique used by Specim-IQ is line-scan or push-broom scan, where one line (row) of image pixels is registered at a time.

Specim IQ: The camera that is used throughout this research work for the purpose of imaging is a camera manufactured by the Finnish company Specim, and is branded under the name Specim IQ. It is a portable HS camera which is functioning with a line-scan hyperspectral imager. The wavelength range of Specim IQ is 400-1000 nanometers. The spatial resolution of the recorded data is 512×512 pixels. The resulting hyperspectral data is a three-dimensional data cube, it provides the user with both spectral and spatial information. In addition to the hyperspectral data, Specim IQ saves also a 5-megapixel color image of the target [14]. This camera has been extensively used in the hyperspectral research landscape for classification purposes and with the incorporation of Machine Learning (ML) algorithms, as in [11]. It has been shown to be comparable with non-portable models in terms of performance.

2.1.3. Illumination

There are three major concepts regarding the light and lighting of the scene.

Illumination Source: The illumination available in the scene for HSI should satisfy two requirements. Firstly, it should cover the whole spectrum registerable by the camera, and secondly, a continuous spectrum without (many) spikes or without high spikes is needed. In outdoor conditions, direct sunlight can also be used. For Specim IQ camera, incandescent light and daylight are the two types of light that are recommended [15]. The shapes of the spectra of different lights are available in Figure 2.6. In [16], a more diverse set of light sources spanning along a longer WL range are available in the relevant diagram.

Intensity: In Machine Vision (MV), the amount of light energy that the camera needs to be exposed to (for proper reflectance registration) will define the intensity of the light needed for the imaging. In HSI, there are numerous internal sensors for capturing the numerous wavelengths. Because of the division of the light between these sensors, more light energy (longer period of exposure) is needed, which is the reason for the relatively long integration time. The effect of lower intensity on the spectral signature is as if the spectral signature curve is compressed from above, as pointed out in [17].

Uniformity: If the light is not spread evenly, the image suffers from unequal luminance, meaning two similar points with one single material may have different spectral signatures when the light is not evenly distributed. It is practically difficult to satisfy, but using the correct positioning of objects in the scene, and controlling the uniformity of light (for instance, illuminating with four lamps instead of only one lamp), is achievable in MV problems [15].

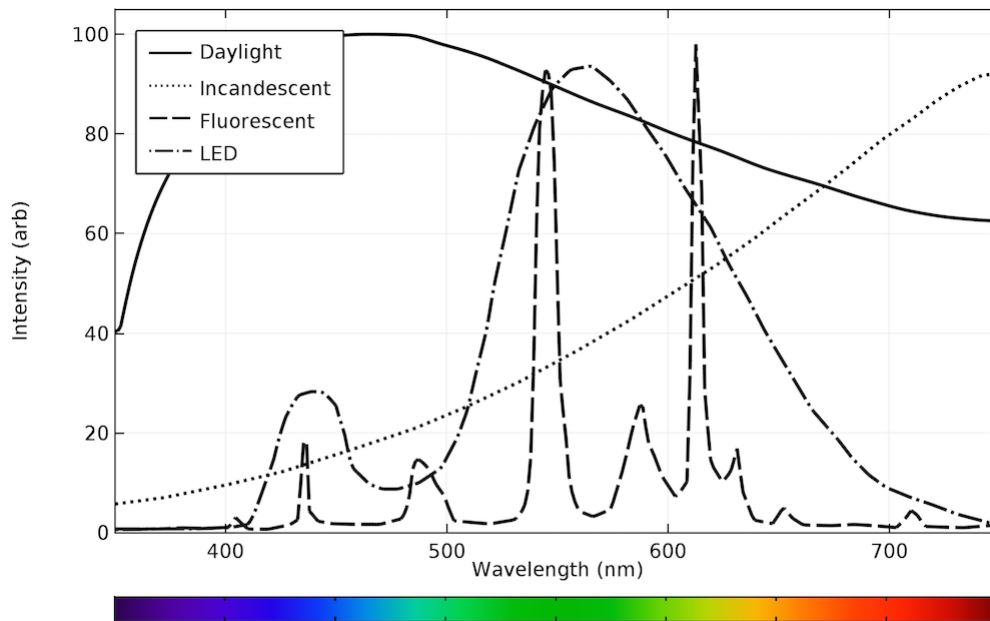


Figure 2.6 Spectra of halogen light from 350 nm to 750 nm wavelength [18]

2.1.4. Setup and the scene

The angle between the axis of the lens of the camera with the normal of the imaging plane can influence the registered data of an image. Specifically, it is important to note that when comparison of two surfaces is a concern, the angles of the camera with the imaging surface in one should be as close as possible to this angle for the other imaging surface. In practice, different results for different angles has been achieved while imaging with Specim IQ camera [11], proving that angle orientation needs to be accounted for when performing HSI [19]. Minimum and maximum distance to the camera may be defined by the manufacturer of the specific device (sensor), but we should consider that if the subject covers more pixels in the image, the overall result is clearer for further processing. For the Specim IQ camera, no maximum distance is mentioned, and the minimum mentioned distance is 15 centimeters from the adjustable lenses of the camera [15]. As a general rule, the camera should not face the light directly

when imaging. It also should not be in a position where the level of light is low. Too low levels of light will affect the quality and accuracy of the image.

2.1.5. Structure of the HS image files

Figure A6 (appendices) clearly shows how the three popular HSI file formats (BIL, BSP, BSQ) store the image file with respect to the order of writing the pixels.

2.1.6. HS Image preprocessing

For smoothing the spectra in HS images, two methods have proved useful in many research works. The simpler one is the "average" filter, and the "Savitzky-Golay" filter. Savitzky-Golay has also been promising when the derivative of the reflectance spectrum is to be used for the matching/training process [20].

2.1.7. History and some applications of HSI

Spectral imaging, and specifically hyperspectral imaging has been known, accepted, and applied for decades, but its availability has been bounded to a very specific range of users and applications. Due to the limitations of regular machine vision and spectroscopic techniques, hyperspectral imaging was developed back in the 1970s [21] when NASA started installing spectral imaging facilities in satellites. This continually increasing spectral image quality paired with the incredible simultaneous advances in desktop computing allowed the application of image processing and statistical analysis, and opened doors for hyperspectral imaging research to flourish [2], and has since had usage especially, in engineering and science fields such as Robotics [22], Mechatronics, Geology, and similar fields [23] [24] [25].

Detection and analysis of vegetation has been carried out in ice and snow conditions [2], in a similar way, there is the potential to perform such analysis for rescue operations, for instance when humans are lost in cold mountain environments and need to be found in a timely manner, or in autonomous vehicles where pedestrians need to be detected for better safety of the system. One method to perform this using hyperspectral imaging is by collecting skin samples [26] and building classification models based on those [27]. Classification methods have been used in this area for the issue of detection [27] and have been contributed to areas like medical diagnosis [28].

Using features such as derivative of the spectra [20] in combination with other methods may allow for optimization of the classification models in regard to their performance.

2.2. Material classification for HSI with the use of ML and SM

Material classification is one of the main purposes of the utilization of Machine Learning (ML) and Spectral Matching (SM) in the scope of hyperspectral images. When performing the classification on a pixel level, the result can be the segmentation of the image, as shown in Figure 2.7, meaning that each pixel will be assigned a specific class, and the image is divided into such classes.



Figure 2.7 Image segmentation using HS images for plum fruit quality assurance [29]

2.2.1. Feature selection

Selecting the features with the most significant influence on the classification process, and thus reducing the number of features will cause the process of training, analysis, and detection/classification to consume fewer resources (become faster), and in some cases will result in the improvement of the identification of a class [30]. Moreover, in cases where the number of features results in an over-fitted model, feature reduction may be a solution. On the other hand, reducing the number of features should be carried out carefully, and should account for the effect of this reduction on the accuracy and overall performance of the model. The method to select the features and the number of reduced features are going to be important factors in the feature selection process.

There are three groups of approaches for the feature selection procedure [31]. The filter method approaches select features regardless of what the model is. When a certain criterion is satisfied they mark a feature as selected. The filter group of approaches has been prominent because of the speed they offer when selection is carried out [32]. With wrapper and hybrid methods, although they might provide better performance of the model overall, the cost of the CPU time is relatively higher in those methods [33]. Aligned with our choice of faster models, filter methods are of preference in this work.

2.2.2. The models

In the methods used for HSI material classification, pixel-wise consideration of the problem is extensively common and useful. In pixel-wise classification, an input data point of the system is the pixel vector R^P (each of whose element $R^P(i)$ is the reflectance value at band i). During the last few years, numerous pixel-wise classifiers have been adapted and applied to HS image classification problems, maneuvering on algorithms such as random forests [34], k-Nearest Neighbors (kNN) [35], Support Vector Machine (SVM) [36] and Artificial Neural Networks (ANN) [37]. Besides, Spectral Matching methods, in which a measure of similarity of spectral signatures is calculated are frequently opted for classification of the pixels according to the reference data point(s). Among SM methods, Spectral Angle Mapper (SAM) [38] has remained performant and actively beneficial throughout the years for HS classification problems [39] [40] due to many facts, such as its tolerance against the lighting condition [38] and the speed it lays out for high-dimensional datasets.

ANN, kNN and SAM have been around for many years [41], and they still play an important role in the current HSI classification literature. Employment of SVM, kNN and SAM classifiers for plant disease and classification on the HSI data has proposed promising functionality of such methods [5]. kNN and the relevant derived models based on kNN have proven to be 95% to 98% performant according to accuracy on the Indian pines dataset for classification [42]. These methods are still flourishing and are comparable to Convolutional Neural Networks (CNN), and except for ANN, they are all faster and need a very short (or no) training/processing time.

2.2.3. Evaluation

After the models are compiled, configured, and run the testing phase starts. It is where the performance of the models is evaluated, which provides the basis to be able to identify how desirable each method outcome acts relevant to our expectations.

Initially, the prediction is carried out on the test dataset, which needs to be different from the training dataset. Through the prediction, data points (pixels) are classified (and labeled) into different classes (two groups for a binary classification problem), and the predictions are then compared to our ground truth dataset, where the actual classes of each data point have been marked. As a result of this comparison, in a binary classification problem, four groups of points can be identified:

- **True Positive (TP):** These are the points that are predicted by the model to belong to the **positive** class, and they actually belong to the **positive** class.
- **True Negative (TN):** These are the points that are predicted by the model to belong to the **negative** class, and they actually belong to the **negative** class.
- **True Positive (FP):** These are the points that are predicted by the model to belong to the **positive** class, but they actually belong to the **negative** class.
- **True Positive (FN):** These are the points that are predicted by the model to belong to the **negative** class, but they actually belong to the **positive** class.

Computing the number of the points in these groups after running the models and compiling the results in one table, leads to the composition of the confusion matrix (Figure 2.8). For the problem of classification (binary or non-binary), the confusion matrix is among the first fundamental entities which are calculated for assessing the classification performance.

		Predicted Class		
		Positive	Negative	
Actual Class	Positive	True Positive (TP)	False Negative (FN)	Sensitivity $\frac{TP}{TP + FN}$
	Negative	False Positive (FP)	True Negative (TN)	Specificity $\frac{TN}{TN + FP}$
		Precision $\frac{TP}{TP + FP}$	Negative Predictive Value $\frac{TN}{TN + FN}$	Accuracy $\frac{TP + TN}{TP + TN + FP + FN}$

Figure 2.8 Confusion matrix together with evaluation measures derived from it, for a classification problem with two classes "Positive" and "Negative"

For the problem of classification, there are several measures of classification performance that may be directly calculated from the confusion matrix. "Accuracy", which defines the total number of correctly predicted points (TN, TP) in relation to the total number of points (TN, TP, FN, FP) expresses how accurate the model is performing

in predicting overall. It is one of the most effective measures in the field [43], specifically, when class imbalance (large difference between the number of data points in each class) is not an issue. Equation (2.3) proved the mathematical formulation.

$$Accuracy = \frac{TN + TP}{TN + FP + TP + FN} \quad (2.3)$$

Accuracy should ideally be 1, which means that FP and FN values are zero and it is not associated with a specific unit. In cases when the dataset is not balanced, the accuracy value may be misleading, and other measures need to be taken into account as well. "Recall" (aka. "sensitivity" or "true positive rate") and "precision" are the other metrics for this purpose [44]. They are formulated as may be seen in Equations (2.4) and (2.5). Equation (2.6) shows how F1 score as a combination of precision and recall is calculated.

$$Precision = \frac{TP}{TP + FP} \quad (2.4)$$

$$Recall = \frac{TP}{TP + FN} \quad (2.5)$$

$$F1\ score = 2 \times \frac{Precision \times Recall}{Precision + Recall} \quad (2.6)$$

The ideal value for precision and recall are also 1, meaning that the FP and FN are ideally zero (respectively). For the F1 score too, a value of 1 is ideally expected.

2.3. Software for HS image analysis and classification

It is only recently with the advent of portable HSI cameras, that this technology began serving numerous users and applications in science, engineering and academia. To complement the hardware aspects of HSI, appropriate software must be made available to researchers and practitioners to satisfy their diverse needs.

Various software applications have been proposed in previous years, but they can be in most cases associated with limitations, imperfections or complexities for amateur portable camera users and novice learners of HSI technology. Some of these tools are designed with only one very specific problem in mind [45]. Some do not offer an easy-to-use interface or do not offer a GUI at all [46], which arise the need for the user to get involved with coding. A number of tools like ENVI are not free, and free GUI tools are usually too basic, even for the needs of amateur engineers. It might also be the

case that the software is outdated [47], discontinued, etc. In many of the cases, the current software tools are linked with more than one of the issues in question. For instance, ENVI is a very comprehensive multi-purpose tool for multispectral imagery, but it is too complicated for the aim of qualitative HSI analysis, necessitates a long learning process, and is not free.

MATLAB, as a development and computation environment, has been, for long, a major player in the landscape of scientific programming [48], and at the same time, it is broadly accepted in academia and education (more than 6500 academic institutions are licensed as claimed by Mathworks in 2022 [49]). There are other features like different deployment methods (such as web deployment), integration of programming and image processing, and suitable handling of image files. These turn MATLAB into one of the most suitable platforms on which our HSI application could be developed, for interdisciplinary, engineering, scientific and educational usages.

2.4. Potential areas of focus (existing gaps)

According to what has been put forward in the previous sections, ongoing work is in progress in the fields involved in material classification and hyperspectral image analysis. Since material identification using HSI has shown to have novel applications in the Mechatronics-related fields (as discussed in 2.1.7), such as medical robots and autonomous vehicles, it is important to specifically apply learning techniques on HSI data for related applications.

It is also crucial in some applications to be able to optimize the model with respect to the specific usage and knowledge of that specific domain. This might be fulfilled through many methods like introducing features such as spectral derivatives for classification.

As a next step, as explained in 2.3 there are vast opportunities toward facilitation of the analysis and processing of hyperspectral images for a general user who does not intend to deal with the complexities of coding, or even be engaged with expensive professional software environments. In that respect, the development of graphical user interface software may provide a solution.

The three mentioned areas of work are specifically becoming important as portable HS cameras are gaining wider availability and popularity during recent years. The three main concerns of this work (expressed in section 1.1) and the three research questions in section 1.3 are in accordance with topics in the three mentioned areas.

3. MATERIAL CLASSIFICATION

The mechanisms and methodical operations involved in the first part of this research work such as understanding and investigating the problem, finding and applying the solution, and evaluation of the results are discussed in this chapter.

3.1. Getting a general picture of the problem

Human skin identification is an instance of a classification problem whose outcomes may be utilized in mechatronics, robotics and related fields including Machine Vision. Hence, although other examples for classification were considered in the progression of this work, human skin classification is chosen as the main problem in this section.

3.1.1. The data points

In the human skin classification problems, there are basically two desired classes to which we would like to classify pixels. One is "skin" which consists of real human skin pixels, and "non-skin" class contains all other pixels including fake skin pixels (fake skin pixels belong to the printed image of human skin which is present on the scene, for instance on a journal cover). Where a reference point is needed or when training needs to take place, data points from one person are used, and when the model is configured, it is applied to another person's image for prediction and test purposes, ensuring that the model has the potential to work on different subjects (different datasets). The following figure is a false RGB (fRGB) representation of our original image. In the figure, the hand of the person on the right is pointed out as the reference set when spectral matching is used, and as the training set when machine learning methods are applied.

The real human skin (arms, hands, necks and faces) is supposed to be classified as "skin" class, and all other pixels in the image, as "non-skin" class. The fake skin pixels (from the man's face and neck, on the cover of the journal) are the pixels that do not belong to a real human in the image and should also be classified under the "non-skin" category. Figure 3.1 exemplifies such points.

Each data point taken from the image may be considered a vector whose elements are the values of reflectance of different bands for a specific pixel. For 204 bands, this vector would be regarded a 204-dimensional vector. Each element of the said vector is considered a feature, and the value of each element (feature) is a 12-bit integer number.



Figure 3.1 The original image upon which the classification takes place

The data cube of the original image is hence of size 512 by 512 by 204.

3.1.2. The patterns in the skin spectral signature

When graphing the spectral signature of sample points (Figure 3.2), unique patterns and trends are observable, which may render the process of classification possible. As

an instance, in real human skin, nearly in all such data points, there exist a “w” shape at WLs from 540 nm up to 585 nm. Besides, the curves related to real skin show an increase from 425 nm to 490 nm, while the fake skin points expose a decrease in this interval.

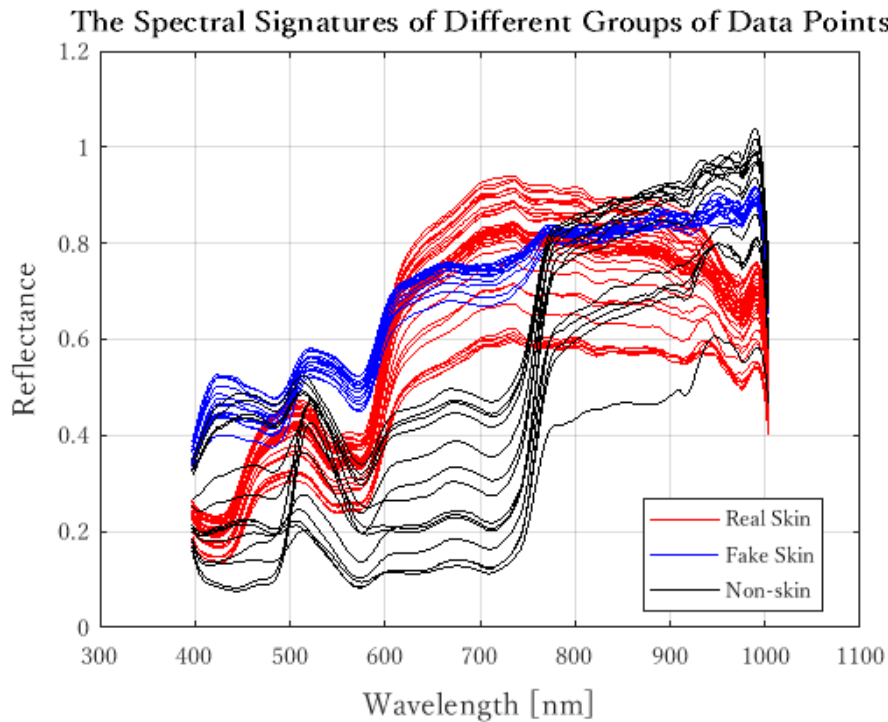


Figure 3.2 Spectral signature of different groups of data points

3.2. Imaging

As a first step, the (imaging) data should be collected. To perform imaging appropriately, there are several parameters to investigate and choose from as discussed in section 2.1.

3.2.1. Imaging parameters

The light source: According to the explanations in item 2.1.3 the best light sources for hyperspectral imagery are natural light (sunlight) and incandescent light. Moreover, due to the applications of hyperspectral imaging that we considered in this work, the subject will be most probably available in open spaces where natural light is the only source of illumination. Hence, the imaging has been carried out under the natural and incandescent light. Figure 3.3 shows how the fingerprint (spectral signature) of human skin looks in the two environments with two different light sources.

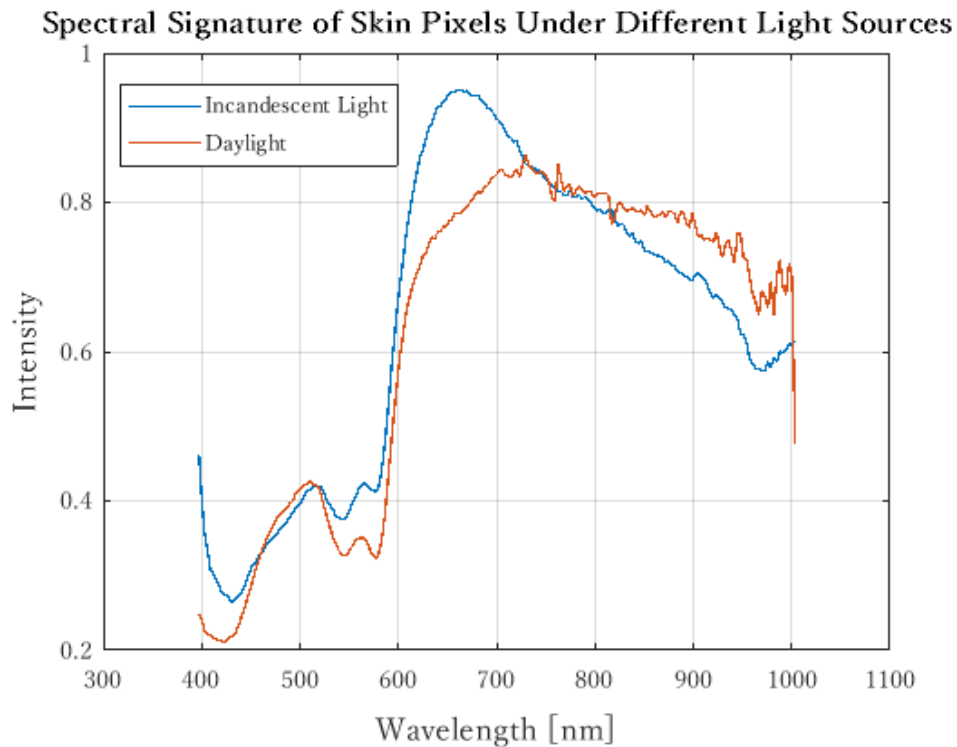


Figure 3.3 The spectral signature of human skin imaged under two different light sources

Intensity: The intensity of the light should be neither very small nor very large in value in order to gain the best results. Too large values will cause saturation and too small values will result in the signature to be more flat [17]. This can be controlled by changing the object-to-source distance under incandescent light as the distance and light intensity has an inverse relation with a power of two [50]. For daylight, by choosing the optimal time of the day for imaging, we may provide proper light for the image capture.

Uniformity: As for the uniformity, in natural light, images were taken in smooth uniform shadows, with no direct sunlight, and during the afternoon and early evening (between 13:00 to 17:00). Under incandescent light, a dark room was selected, and a distance of approximately 1 meter existed between the subject and the lamps. The lamps were oriented at 45 degrees angle to the subject.

Camera orientation and position (angle and distance): Based on the recommendations of the manufacturer [15] (visible in the next figure), the best results are achieved when the camera is oriented at an angle as close as possible to 90 degrees with subject's surface. Hence, the attempt was to achieve photos with such a condition, but the angle parameter did not tremendously influence the final spectral signature and the final classification results with angles close to 90 degrees.

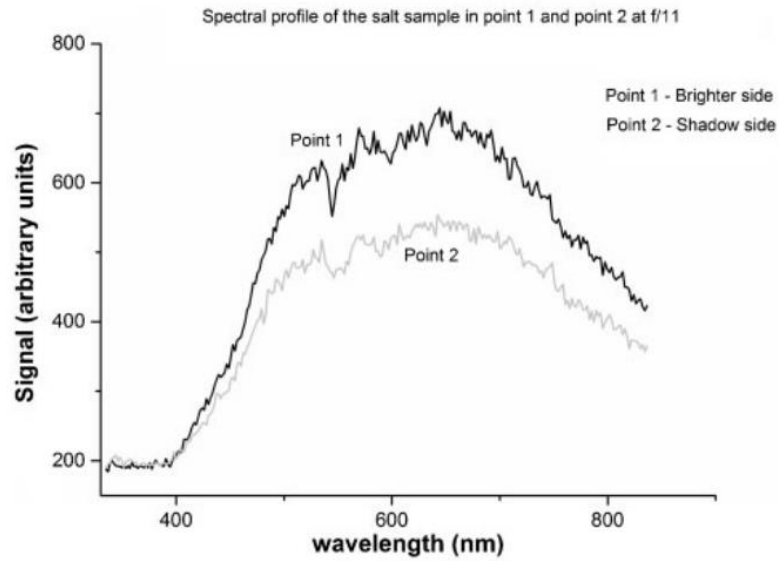


Figure 3.4 Two points of an object which are exposed to different light intensities[17]

The distance between the imaging subject and the camera affects the accuracy of the spectral signature and the number of data points of a classification group in the image. Distances less than 100 centimeters and more than 300 centimeters did not prove to be useful for our purposes.

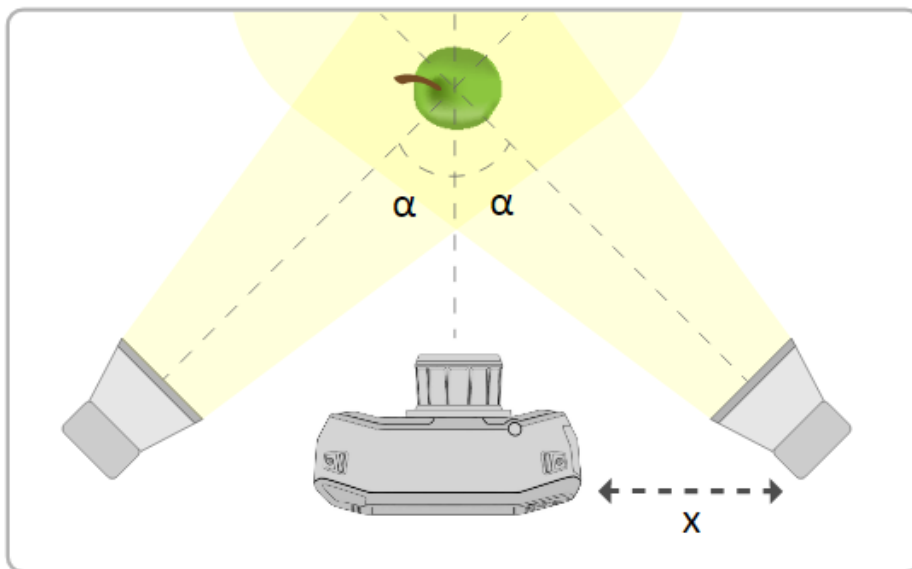


Figure 3.5 An ideal camera/lighting positioning/orientation suggested for the Specim IQ camera by the manufacturer. X should be larger than 15 cm, α should be close to 45 degrees, and the distance of the camera's lenses to the object should not be less than 15 centimeters. [15]

Integration time: The integration time indicates the amount of time that the sensor is permitted to gather light photons. The higher the integration time, the more photons the system collects for each wavelength, which usually leads to higher intensity. As a general rule, when there does not exist sufficient light, the integration time should be higher to collect enough photons, and as the light source intensity goes higher, less integration time is needed. For the image acquisition experience of this work, integration times between 60 seconds up to 180 seconds were opted. The camera offers an automatic suggestion for the integration time, but manual intervention is needed from time to time as the suggested time does not always produce the optimal results.

Imaging Subject: The imaging subject is the skin of different parts of the body of human subjects.

White reference: The existence of a specific pad with specific material as a white reference has been considered in this work. This pad is included as Specim IQ camera's accessories. Image element white references have also been considered (such as snow), but the best result is achieved with the specific pad.

3.2.2. Selected imaging parameters

A summary of the final selected parameters in tabular format is expressed in Table 3.1.

Table 3.1 Summary of imaging parameters used

Parameter	Natural light	Incandescent light
Light source type	sun's uniform light	two incandescent lamps
Light source distance to subject	inf.	~ 1 meter
Light source orientation	spread uniform light	spread direct (45 degrees)
Other light source conditions	taken between 13:00 and 17:00, in smooth light/shadow	dark room
Distance to camera	1-3 meters	60-120 centimeters
Camera's angle (to surface perp.)	70-90 degrees	60-80 degrees
Integration time	60-180 seconds	90-180 seconds
White reference	White reference pad	Included in accessories

3.2.3. Camera calibration

For the imagery, calibration happens on two different levels. The calibration of the camera has to be performed in each environment when the type of the light source changes or the intensity of the light goes under significant change. This is a partially automatic procedure that needs to be performed via the camera's setting and before starting the imaging. For the Specim IQ camera, the calibration may be carried out using calibration and reference pads accompanying the camera as instructed by the manual. The second level of calibration (calibration of the image) is made possible with the white reference pad, and the related calculations are discussed in more detail in 3.4.1.

3.2.4. The setup

There are two imaging setups considered throughout this work. The imaging setup related to the development of the models in this chapter is illustrated in Figure 3.6. The other imaging setup, in which the light source is incandescent lamps, together with some acquired images in that setup is visible in Figure A7 (appendices). Skin samples are taken from 3 human subjects and it is possible to see a number of the samples in Figure A8.

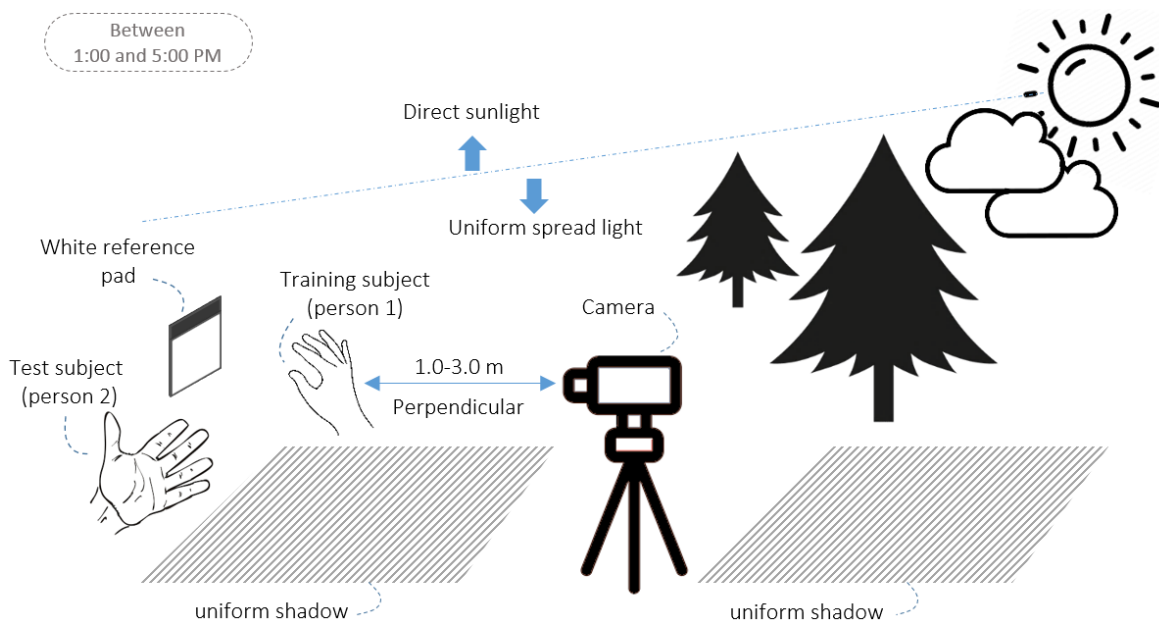


Figure 3.6 The imaging setup used in natural light

3.2.5. The summary of the process

In short, the imaging process follows the steps illustrated in Figure 3.7.

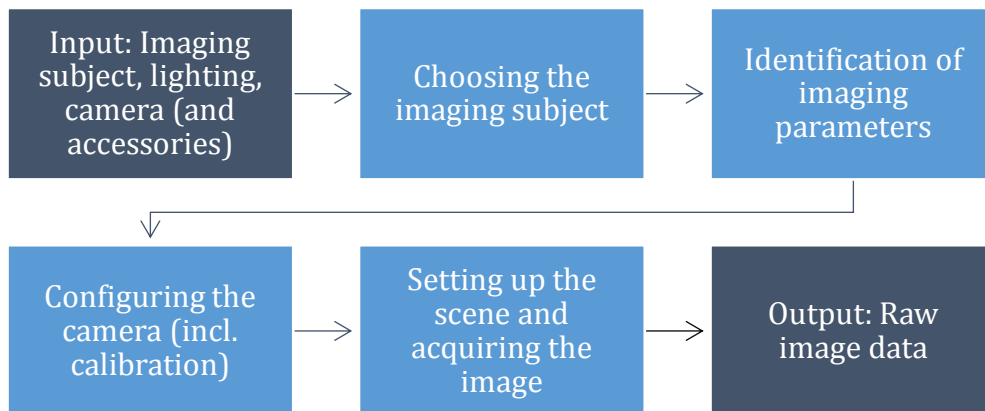


Figure 3.7 Summary of the steps involved in imaging

3.3. Dataset

As explained in 3.1.1, our dataset consists of data points in two main classes, “skin” and “non-skin”. In this section, different concerns about the dataset are put forward.

3.3.1. Number of training instances

The number of instances used for the purpose of training, for a single class in pixel-wise classification can largely vary such that values as low as 200 instances for a class can be successfully used [51] [52], and, based on the method’s choice, values may increase higher [53] to gain higher accuracy. The number of the data points used in different experiments in this work ranges between 500 and 10000 instances for each class.

3.3.2. Class balance

Class balance is a measure that specifies how close are the number of training points between different classes (balance). The balance of classes may have an effect on the training process and is influential to the evaluation process of machine learning methods. We may use up-sampling or down-sampling if class imbalance occurs. Since we have control over choosing of our samples, we can make the decision about which pixels to image and which pixels to select. Therefore, the imbalance is not in most cases a concern for us, but in case it was needed, up-sampling is applied to the dataset.

3.3.3. Variety

To be able to apply the model for different scenarios, it needs to be tested and trained on the material data of an entity in its different varieties. For instance, if the focus is classification/detection of the human skin, then the skin of more than one body part should be taken into account for test (e.g. skin of forehead, cheeks, forearm, and hand) to make a proper evaluation. Moreover, the skin of people with different skin colors should be brought into the experiments to avoid bias as much as possible. For the purposes of this work, spectral signatures of the skin of five persons with various skin tones were captured and some of that data was used in the training process after review.

3.4. Preprocessing

Prior to the development of the models, our data (spectral signatures of the pixels in the image) should undergo different operations to provide the possibility of a more accurate analysis of data. Since this phase is happening before the main processing of the data (applying the models and performing evaluation), it is named preprocessing in MV and ML literature.

3.4.1. Image calibration

Calibration of image pixels is carried out to eliminate the effect of the light source spectrum on the registered material spectral signature. It is a type of normalization of pixels spectrum with the "Dark Reference" as the lower end, and the "White Reference" as the higher end. The next equation is expressive of the operation.

$$R^{image} = \frac{I - D}{W - D} \times 100 \quad (3.1)$$

Here, R^{image} shows the reflectance values of the calibrated image. I is the original image matrix containing raw reflectance values, D is the dark reference image, and W represents the white reference image, which should both be the same size as I .

3.4.2. Imputation, numerical encoding

Since our input data in the dataset is comprised of data points from an image, gaps, null values or values of improper type (numerical, categorical, etc.) are not going to be a concern. All the values are floating point (continuous) decimal numbers. There is

hence, no need for data type conversion or any numerical encoding, nor is there any need for caring about the gaps and null values in our case, since all pixels in all the bands have values recorded.

3.4.3. Filters

For various reasons including the presence of the effect of noise on the reflectance values, the shape of the spectral signature is affected and is not appropriate for analysis and gaining optimal information. To this end, two smoothing filters were reviewed, and one of them was selected and applied to all image pixels for further operations. The first filter is the Savitzky-Golay filter, and the second one is the Average value filter. The result of applying Savitzky-Golay can be observed in Figure 3.8 (right). The result of applying the average filter is displayed in Figure 3.9 (right).

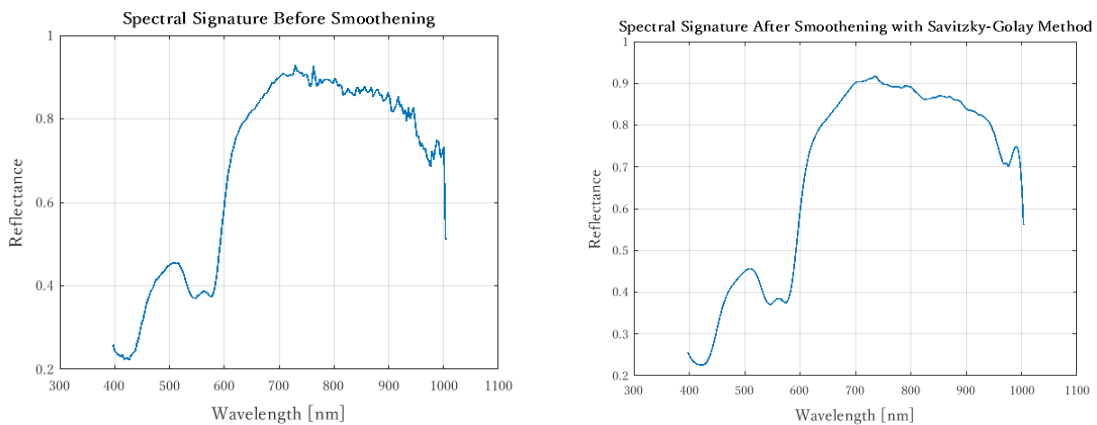


Figure 3.8 Spectral signature before applying Savitzky-Golay (left), and after applying it (right)

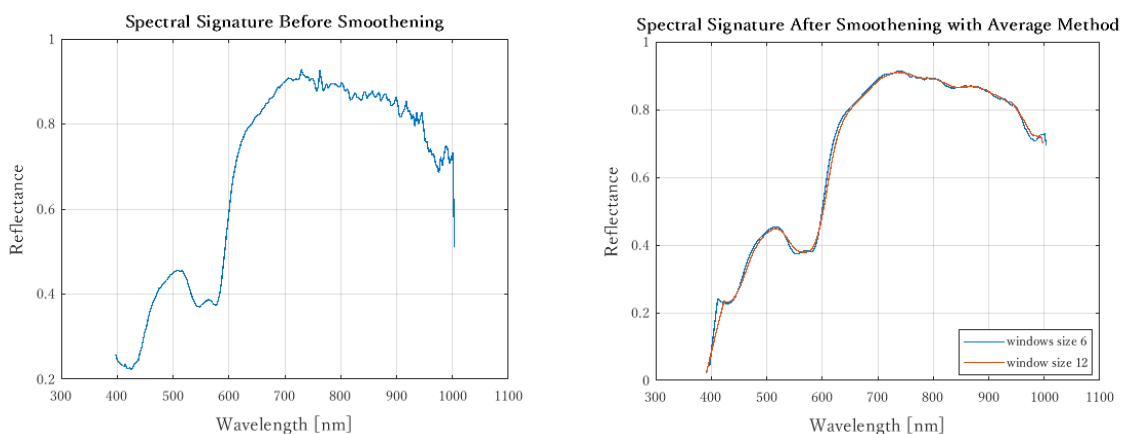


Figure 3.9 Spectral signature before applying average filter (left), and after applying it (right)

Savitzky-Golay is finally chosen as the method for smoothing the spectral signature.

3.4.4. Outliers

In the case of pixel-wise classification, when the training instances are visually selected from acceptable points, the probability of outliers existing is very low, but it might be possible that on a specific texture like skin, entities like moles are present, or observing brown spots on fruits skin as a result of oxidation is common (Figure 3.10). These types of outliers may be avoided to a high degree by careful selection of training pixels.



Figure 3.10 Two kinds of abnormalities on human skin and on fruit skin resulting in outlier points

To verify that we have selected a uniform area of the skin without impurities, qualitative inspection of the selected training points may help. Figure 3.11 shows the pixels which were selected as skin in our experiments. It is observable that the values are not falling out of the specific range of the lowest and highest spectral curves (at least by a large degree).

3.4.5. Normalization

Normalization can be applied in different ways [54]. The normalization which proved to be the most effective takes the maximum and minimum values of each band into account. On a pixel level it is formulated as Equation (3.2):

$$R_{norm}^P(i) = \frac{R^P(i) - \min(R^{band}(i))}{\max(R^{band}(i)) - \min(R^{band}(i))} \quad (3.2)$$

Where $R^{band}(i)$ is the two-dimensional array of reflectance values of all points at band i , $R^P(i)$ is the reflectance value of point P at band i , and $\min(\)$ and $\max(\)$ are the regular minimum and maximum functions applied to the intensity of all pixels in a band.

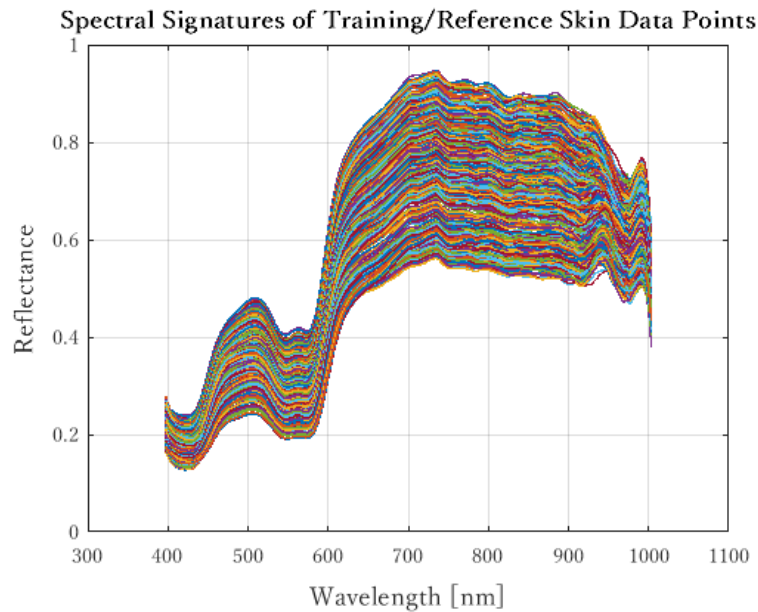


Figure 3.11 Spectral signatures of all the selected skin pixels as training/reference data

3.4.6. Selected preprocessing operations

A summary of the final selected parameters can be expressed as is in Table 3.2.

Table 3.2 Summary of preprocessing steps that were taken

Process	Final Choice	Description
Calibration	Using the white and dark references data	White comes from the white reference pad.
Filters	Savitzky-Golay	Window size = 13, degree = 4
Imputation, numerical encoding	None is needed	No missing data, data is all numeric
Outlier detection	Proper selection of pixels to avoid outliers	Skin pixels without impurities are chosen
Normalization	Max/Min value of intensities in each band	-
Up-sampling / Down-sampling	Proper selection of the number of pixels in each class	In training, the size of the classes should not largely differ

3.4.7. Summary of the preprocessing operations

A summary of the operations carried out during the preprocessing phase is available in Figure 3.12.

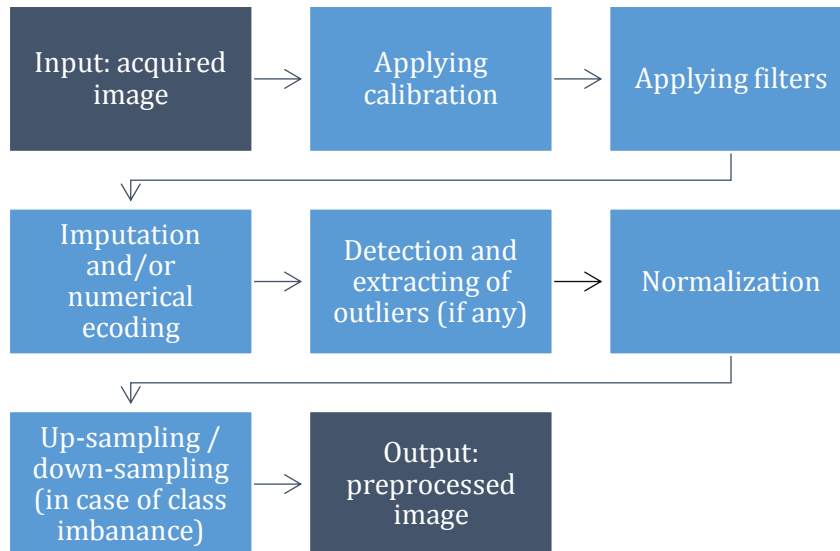


Figure 3.12 Summary of the steps involved in the preprocessing

3.5. Selecting the features

Two different feature reduction methods are chosen to be examined for the detection process alongside performing the process without the use of reduction. The two methods applied use the variance (variance in one class, and variance between classes), and local extrema as indicators of important information for making the selection of most informant features. The resultant set of features contains 2 or more bands in the end.

To gain a general picture and discover if the reduction of the bands may perform well for the process of identification, after the initial selection of the bands, a qualitative assessment may happen. In the next part, a qualitative method, based on feature space visualization is incorporated. Three sample bands are selected as features.

3.5.1. The influence of feature selection

We visualize in the feature space (where axes are selected features) the data points with 3 of their selected features. A few sets of features are examined until the test is passed. We focus on "skin" and "non-skin" data points, and each class is illustrated with a certain color. If the two groups are possible to be distinguished by eyes, then the

qualitative test is passed, meaning that it is much more probable that the distinction will happen through quantitative models when all data points are analyzed. As observed in Figure 3.13 the data points of the two groups are clearly distinguishable by the eyes.

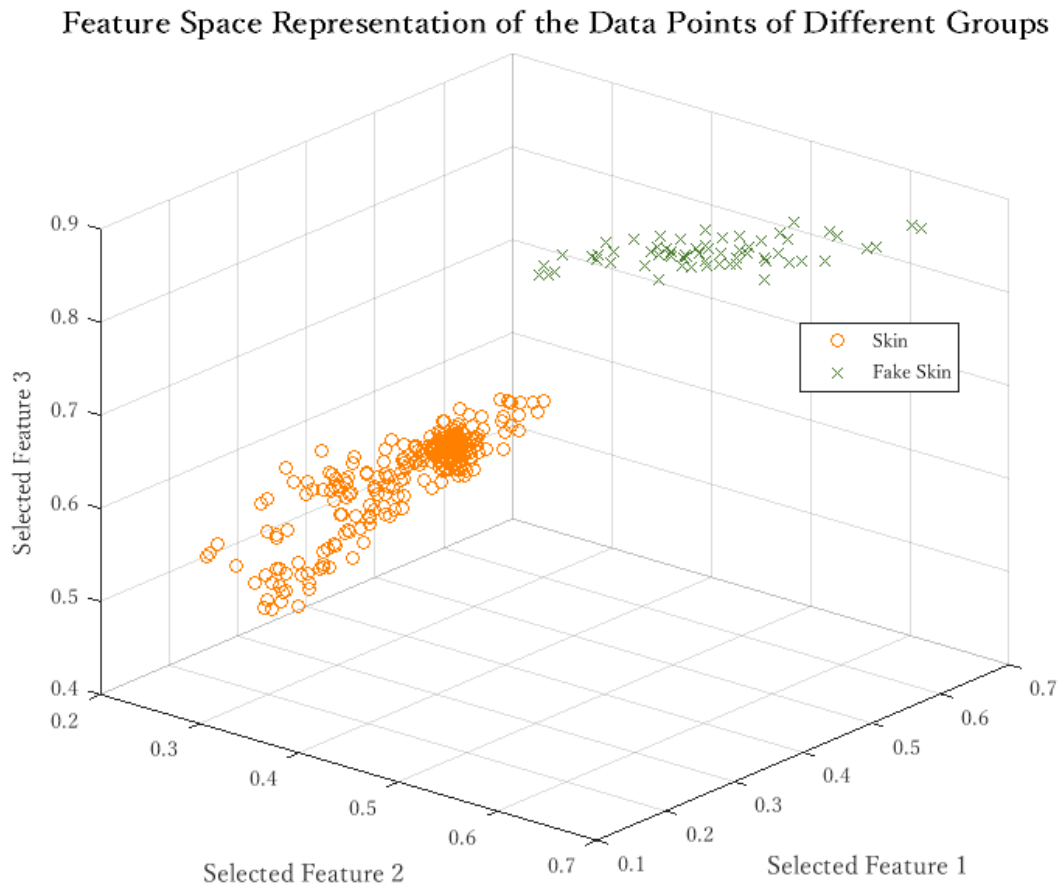


Figure 3.13 Data points of two classes in feature space after feature reduction

3.5.2. Different choices

There are many options for the method to select a subset of the bands that leads to a minimum loss of information and/or improve the accuracy of the classification process. We have chosen two methods belonging to the "filter" group of feature selection methods, and finally, a combination of bands from both methods was opted.

3.5.3. Local extrema

The method of "Local Extrema" pays attention to the bands whose corresponding reflectance values are higher or lower compared to their neighboring bands. For each

material, based on the spectral signature, a specific set of bands will result. For human skin, as Figure 3.14 represents, the local extremum values may be found at wavelengths 419 nm, 510 nm, 545 nm, 565 nm, 582 nm, 725 nm, 975 nm, 990 nm. Some of the extrema may be neglected as they are not relatively high or low in value.

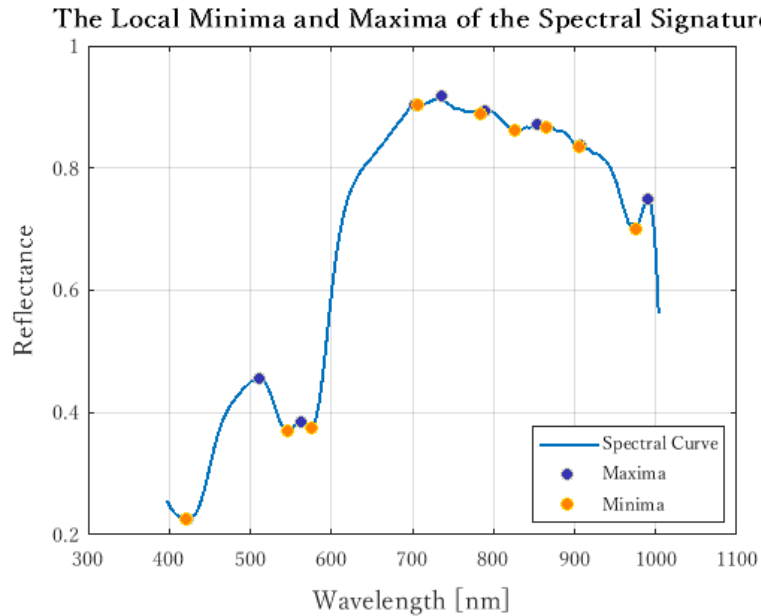


Figure 3.14 The local minima and maxima of the spectral signature of skin pixel.

3.5.4. Using variances

In this method, a feature's total variance (variance over all data points) is compared to the variance of the feature over the data points of each of the classes (variance within each class). If such a ratio is calculated to be high relative to the same ratio for other features, that specific feature is selected, as it has the potential to represent significant information for the classification of the data. The variance of a feature (at band B) over all the points is expressed in Equation (3.3):

$$V_B^{all} = \frac{\Sigma(R^i(B) - \overline{R(B)})^2}{N - 1} \quad (3.3)$$

$R^i(B)$ denotes the value of reflectance of a single data point i at band B . $\overline{R(B)}$ is the mean of the reflectance values of all data points in the whole dataset at band B , and N is the number of all the data points. Then the within-class variances come as Equation (3.4).

$$V_B^c = \frac{\Sigma(R^i(B) - \overline{R^c(B)})^2}{N_c - 1} \quad (3.4)$$

$R^i(B)$ denotes the value of reflectance of one data point belonging to class C at band B . $\overline{R^c(B)}$ is the mean of the reflectance values of all data points in class C at band B , and N_c is the number of data points in class C . Next, the ratio in Equation (3.5) is calculated for all the features, and the bands corresponding to the highest values are selected. Based on this method, the bands with WL 422 nm, 539 nm, 975 nm, 989 nm are chosen.

$$V_B^{ratio} = \frac{V_B^{all}}{V_B^{c1} + V_B^{c2}} \quad (3.5)$$

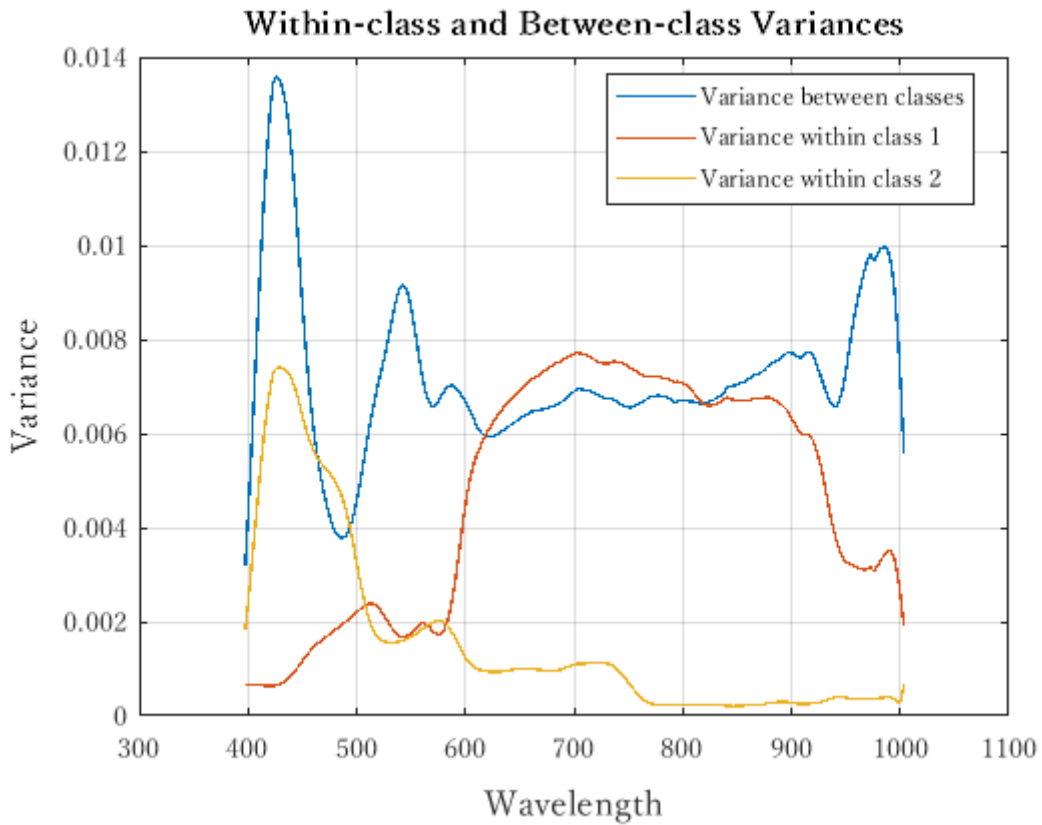


Figure 3.15 Variance between the classes and inside each class in selected dataset

3.5.5. Summary of the feature selection operation

The following figure puts forward, in summary, the general process of feature selection.

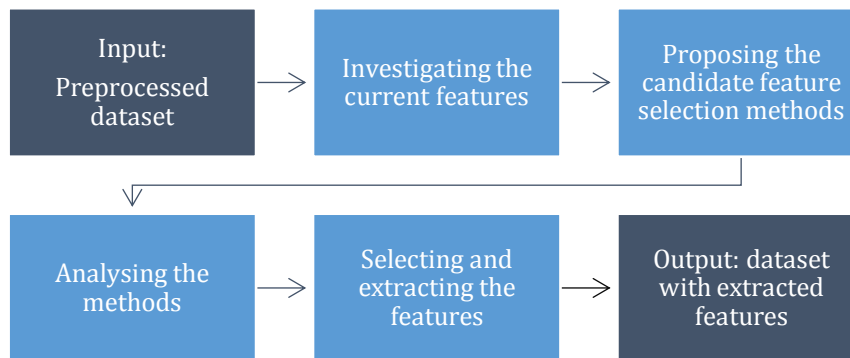


Figure 3.16 Summary of the steps involved in feature selection

3.6. Selecting the models

Based on the explanations in chapter 2 (2.2.2), different models with different mechanisms were considered for applying to our classification problem. There are two major groups of methods. The first group classifies pixels based on their spectral patterns' similarity with the spectral pattern(s) of certain reference pixel(s), and in the second group, a pattern from a selected training set of pixels is learned through popular computer learning methods.

There are four algorithms explored in the first group. These algorithms take into consideration the feature space where each axis represents one of the features (reflectance or 1st derivative of reflectance of the spectral bands), and investigate the closeness of data points with a certain combination of distance measures in this space. In these methods, the model can be identified by:

- The feature type, which can be the reflectance value or the 1st derivative of the reflectance value of a spectral band.
- The selected features (bands), which may be all bands or selected bands.
- The distance measure, which may be the angular or Euclidean distance or a mixture of the two [55].
- The threshold, which is a continuous decimal quantity identifying the borderline that discriminates between accepted and not accepted pixels in a class.

In the second group, two popular machine learning methods are applied to the image pixels, namely k-Nearest Neighbours (kNN) and Artificial Neural Networks (ANN). In these methods, the model can be identified by:

- The feature type, which can be the reflectance value or the 1st derivative of the reflectance value of a spectral band.
- The selected features (bands), which may be all bands or selected bands.
- Model-specific parameters, which are specific to each model. For ANN, the number of hidden layers, and for kNN, the number of neighbors (k) is in this group
- The threshold, which is a continuous decimal quantity identifying the borderline that discriminates between accepted and not accepted pixels in a class.

These six methods have been selected/compiled based on the literature review, the initial analysis, the initial results achieved, and the main purposes of this study.

3.7. Applying the models

In this section, the six pointed-out methods are going to be explained in more detail and the result of the classification on the image will be revealed. Figure 3.17 may be observed as a categorization of the methods according to their mechanism.

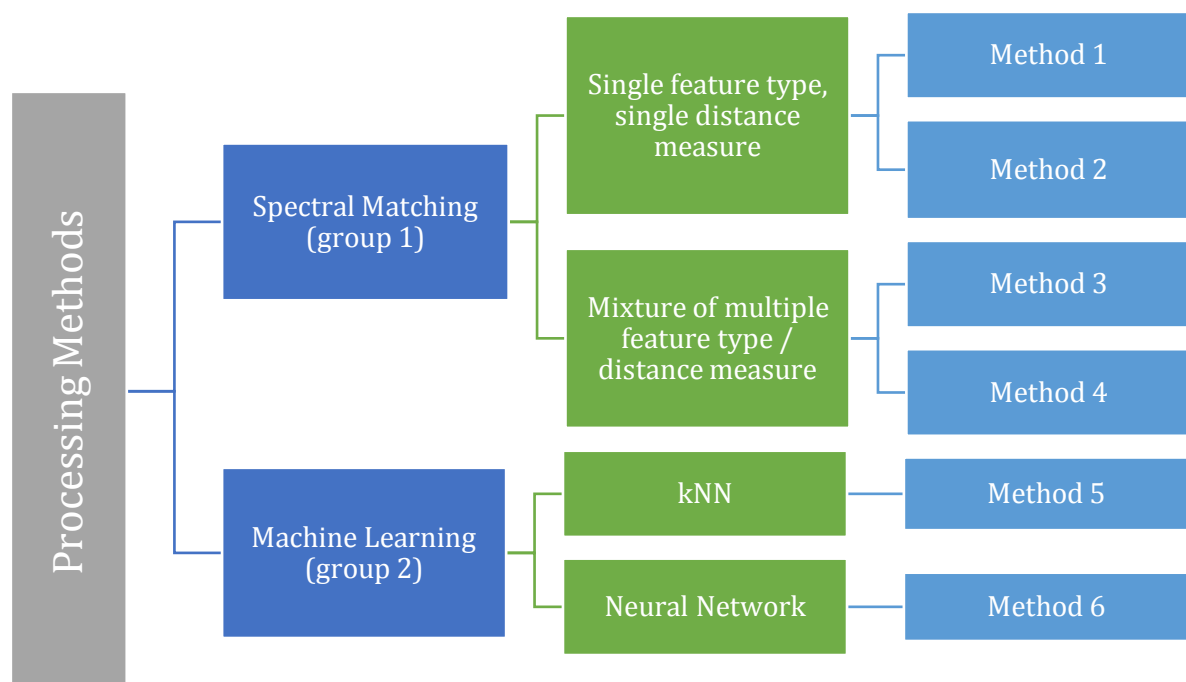


Figure 3.17 Categorization of the methods based on the general mechanism

3.7.1. Method 1: Spectral Matching (SM) using Spectral Angle Mapper (SAM)

In the method of Spectral Angular Mapper, the distances of all the points (P_s in Figure 3.18) in the image with the reference point (P_{ref} in Figure 3.18) is the measure of similarity and is used for the matching process, while each point can be considered as a vector whose elements are reflectance values at selected bands (selected features) in that pixel.

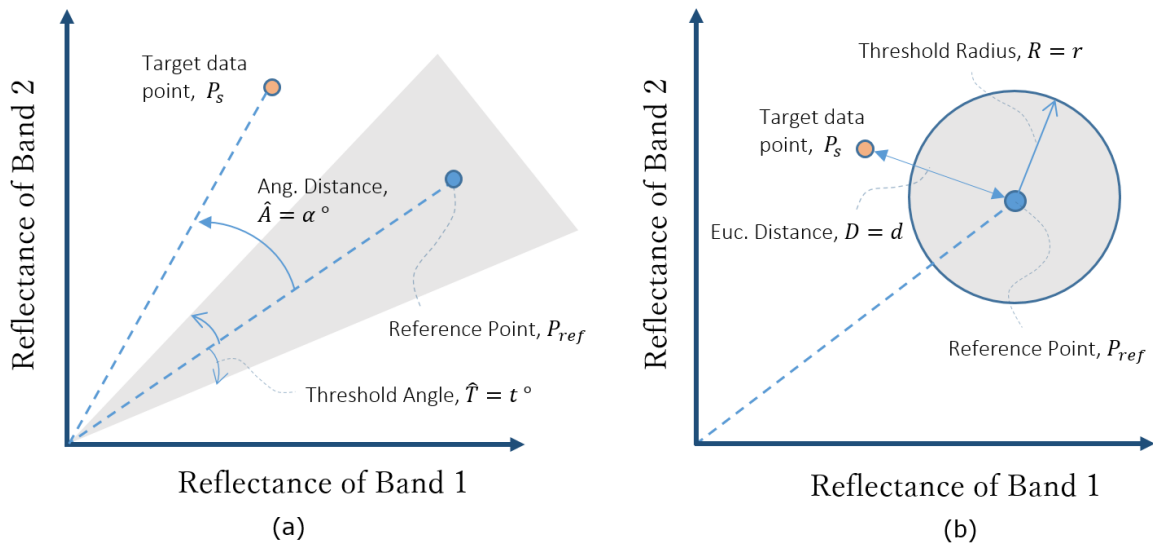


Figure 3.18 Schematic view of methods in feature space. Method 1 (a), method 2 (b)

The following equation expresses the calculation of the distance value for each of the data points with respect to the reference point [38].

$$A(P_s, P_{ref}) = \alpha^\circ = \cos^{-1} \left(\frac{\sum_{i=1}^{N_b} P_s(i) P_{ref}(i)}{\sqrt{\sum_{i=1}^{N_b} P_s^2(i)} \sqrt{\sum_{i=1}^{N_b} P_{ref}^2(i)}} \right) \quad (3.6)$$

$P_s(i)$ denotes the reflectance value of the point P_s at band i . Similarly, $P_{ref}(i)$ denotes the reflectance value of the point P_{ref} at band i . The total number of the selected bands is expressed by N_b . α° is calculated in degrees in our calculation, and may be converted to radians or other angle units without affecting the generality of the solution. After the selection of the referenced point, the threshold needs to be set. This can be evaluated by calculating the range of the angular distance values of a sample set of skin pixels to the reference point. Figure A9 (appendices) shows the range in which this angular distance changes.

When the model is run on the image (taking pixels' spectral signature as input), the values which are going to be accepted as "skin" are the values that are in a proximity of the reference pixels with an angle less than the threshold in the feature space. They belong to the predicted "skin" (or "positive") class, and the rest of the pixels belong to the "non-skin" (or "negative") class. This can be formulated as follows in Equation (3.7):

$$S_{true} = \{P_s \mid A(P_s, P_{ref}) < t^\circ\} \quad (3.7)$$

The figure below shows the result of classification using method 1. The pixels identified as skin are visible in red.

We observe as the result of this classification, that although the method of spectral angle mapper is not very sensitive to the illumination [56], the areas of the arm (the wrist and above) which are not properly illuminated are not detected using the chosen threshold. If the threshold is lowered, allowing for more FN points to be captured, then the FP points will also rise even in larger amounts, weakening the performance of the model.



Figure 3.19 Points classified as skin in method 1

3.7.2. Method 2: SM using Euclidean distance

In method 2, the Euclidean distances of all the target points (P_s in Figure 3.18 (b)) in the image with the reference point (P_{ref} in Figure 3.18 (b)) is the measure of similarity and is used for the matching process, while each point can be considered a vector whose elements are reflectance values at selected bands (selected features) of that pixel.

Equation (3.8) expresses the calculation of the distance value for each of the data points with respect to the reference point.

$$D_{Euc}(P_s, P_{ref}) = d = \sqrt{\sum_{i=1}^{N_b} (P_{ref}(i) - P_s(i))^2} \quad (3.8)$$

$P_s(i)$ denotes the reflectance value of the point P_s at band i . Similarly, $P_{ref}(i)$ denotes the reflectance value of the point P_{ref} at band i . The total number of the selected bands is expressed by N_b . α is calculated in radians in MATLAB, and may be converted to degrees or other angle units without affecting the generality of the solution.

After the selection of the reference point, the threshold needs to be set. This can be evaluated by calculating the range of the Euclidean distance values of a sample set of skin pixels to the reference skin point. A process similar to Method 1 may be used for this purpose.

When the model is run on the image (taking pixels' spectral signature as input), the values which are going to be accepted as "skin" are the values that are in a proximity of the reference pixels with an angle less than the threshold in the feature space. They belong to the predicted "skin" (or "positive") class, and the rest of the pixels belong to the "non-skin" (or "negative") class. This can be formulated as follows in Equation (3.9).

$$S_{true} = \{P_s \mid D_{Euc}(P_s, P_{ref}) < r\} \quad (3.9)$$

Figure 3.20 shows the result of classification using method 2. The pixels identified as skin are visible in red. We observe that many of the skin points are missing in the identification, and many non-skin points are predicted to be of skin class in this method. Therefore, the overall performance is not acceptable as it is later discussed in section 5.1.



Figure 3.20 Points classified as skin in method 2

3.7.3. Method 3: SM using a mixture of distance measures

If we simply merge the results of running the two previous models by selecting the intersection of the true predictions of each model (S_{true}), the true predictions of the third methods can be computed. In other words, the pixels labeled as “true” skin pixels, are the pixels:

1. Whose intensity values are in the neighbouring Euclidean distance of the intensity of the reference point(s) (with a neighboring threshold of R), and
2. Whose intensity values are in the neighboring angular distance of the intensity values of the reference point(s) (with a neighboring threshold of T)

Figure 3.21 shows the schematic of this procedure and Equation (3.10) puts the mentioned mechanism into perspective.

$$S_{true} = \{P_s \mid D_{Euc}(P_s, P_{ref}) < r \wedge A(P_s, P_{ref}) < t^\circ\} \quad (3.10)$$

Figure 3.22 shows the result of classification using method 3. The pixels identified as skin are visible in red.

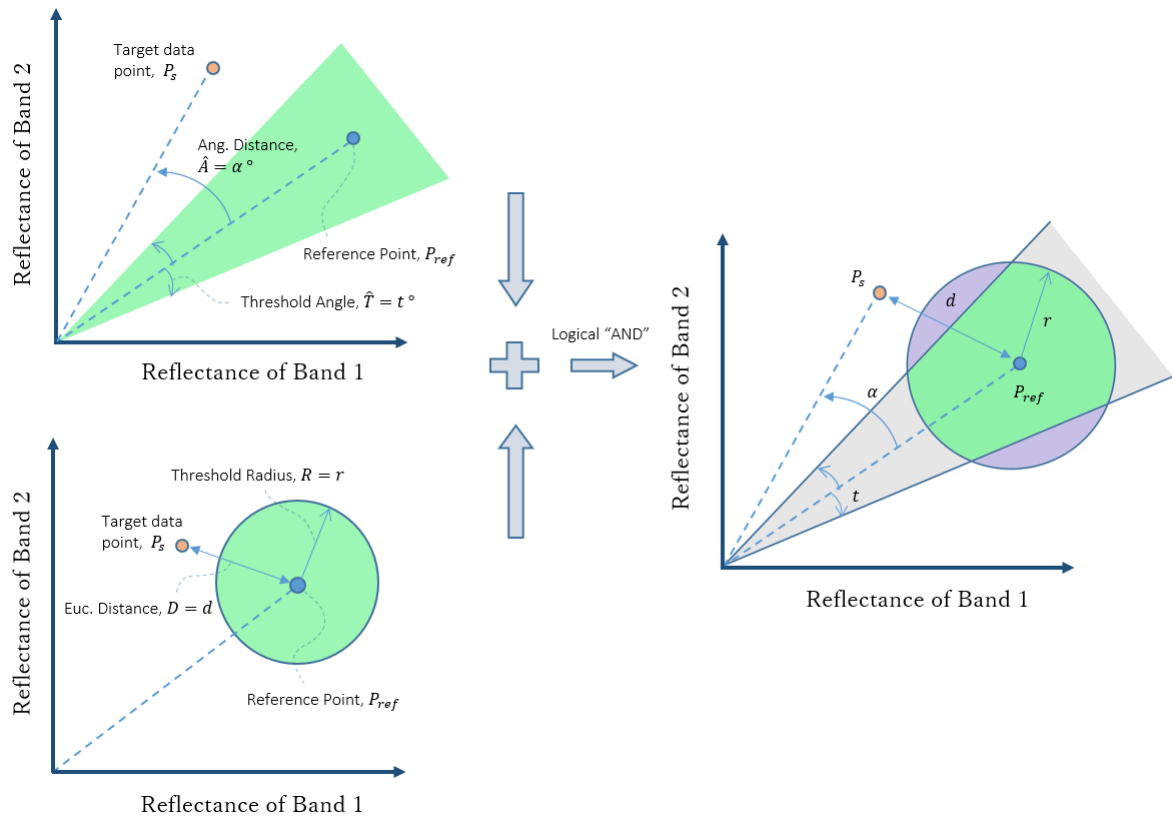


Figure 3.21 Schematic view of the third method's feature space (features are reflectance values)



Figure 3.22 Points classified as skin in method 3

3.7.4. Method 4: SM using a mixture of feature types and distance measures

In this method, the derivative of the intensity (reflectance) values together with the intensity values are considered as features. The accepted results are the data points:

3. Whose derivative of the intensity values are in the neighboring Euclidean distance of the intensity derivative of the reference point (with a neighboring threshold R), and
4. Whose intensity values are in the neighboring angular distance of the intensity values of the reference point(s) (with a neighboring threshold T)

The next equation defines the set of points predicted as the “true” class by this method and Figure 3.23 lays out a schematic view of the feature space.

$$S_{true} = \{P_s \mid D_{Euc}(P'_s, P'_{ref}) < r \wedge A(P_s, P_{ref}) < t^\circ\} \quad (3.11)$$

P'_s and P'_{ref} are the spectral 1st derivatives of the points P_s and P_{ref} .

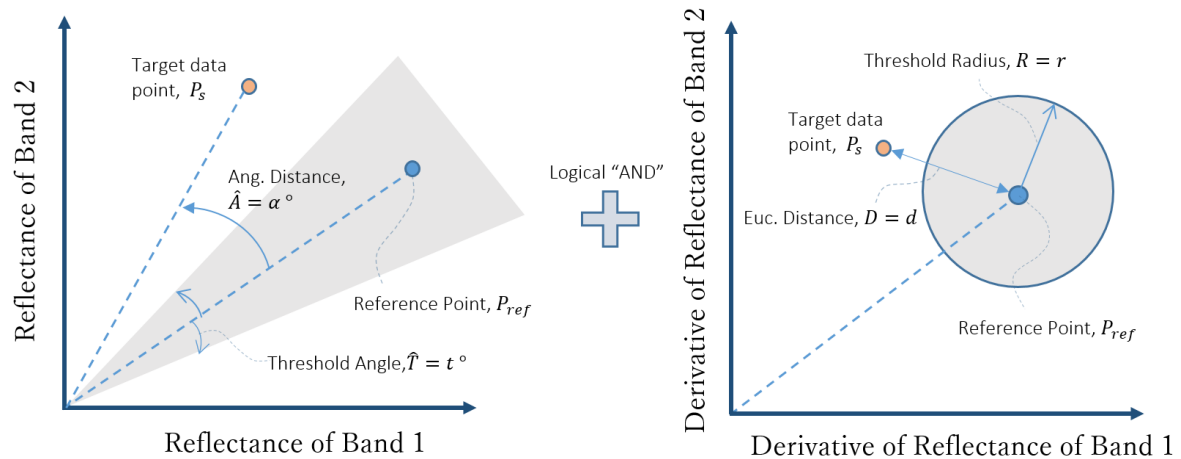


Figure 3.23 Schematic view of the fourth method’s feature space (features are reflectance values, left, and 1st derivative of the reflectance values, right)

In Figure 3.24, the derivative spectra of three groups of the data points are seen. It is obvious how the derivative of reflectance values is making a distinction between three groups at some bands (e.g. at WL of 750 nm). At this band, the reflectance values are overlapping and do not reveal significant information, but derivatives are very different at this band, revealing significant information. Figure 3.25 shows the resulting image.

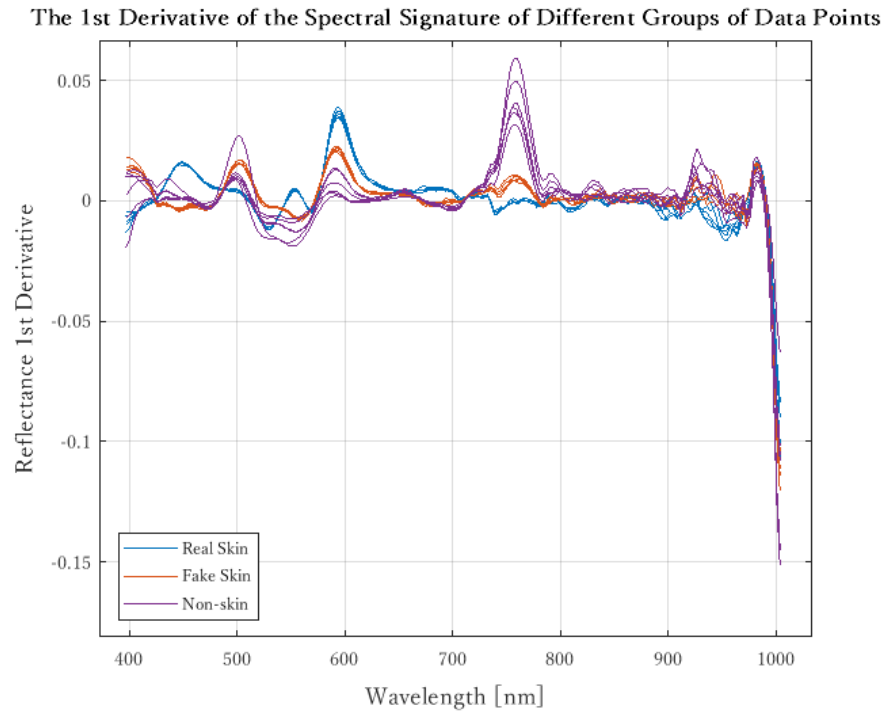


Figure 3.24 The derivative of the spectral signature of three groups of points



Figure 3.25 Points classified as skin in method 4

The spectral derivatives is considered to be calculated and used as a feature in this method since it shows trends in the data, that are not clearly mentioned by the reflectance values themselves. Many interesting features which are unique to a material

are discovered when considering the derivatives, specifically in places where the overlapping occurs in a specific band between the spectral signatures of two different materials.

The derivatives also cause the method to be more insensitive to various illumination intensities, which might be very common as is constantly a concern in hyperspectral imaging because of the angles of the object, presence of clouds when imaging under the natural light, etc. [57].

3.7.5. Method 5: K-Nearest Neighbors (kNN)

In the method of k-Nearest Neighbors, as the name suggests, a number of data points (k data points) with the closest distance to the target data point are computed, and based on the majority voting of their class labels, we can assign a class label to it.

The features that are selected are reflectance values, the measure of the distance that is chosen is the angular distance, and data points are similar to the previous methods. In Figure 3.26 the closest data points to the target (sample) point when $k_t = 3$ are the two points from the red class and one point from the blue class. Hence, based on the majority of the red class points in proximity of the target, kNN classifies target as red class. When this process repeats for all the pixels in the image, the pixels are classified.

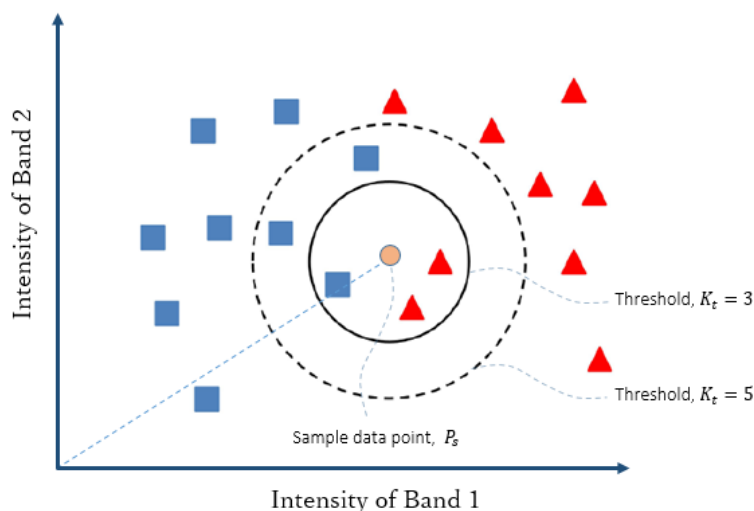


Figure 3.26 Data points in the feature space of intensities in kNN, and the sample (target) [58]

Figure 3.27 shows the result of classification using method 5. The pixels identified as skin are visible in red. Table 3.3 shows different parameters of this method.

Table 3.3 Specifications of the kNN model (Method 5)

Method Element	Value
Features	15 selected features (reflectance values bands)
Distance measure	Angular distance
Class assignment method	Majority vote
Threshold (k)	5
Type of learning	Supervised Learning (SL)



Figure 3.27 Points classified as skin in method 5 (kNN)

3.7.6. Method 6: Artificial Neural Network (ANN)

Artificial Neural Networks (ANNs) have been for long used in classification applications. As the final method of computer learning, they were chosen to be applied and examined as their method of work is unique and expose different features like non-linearity, investigation of trends in the data, and the ability to recognize complex patterns in the data.

In the feed-forward neural networks that we have considered, the selected features of each data point (15 features) are used as the input of the network, then through the assignment of weights and biases, and applying activation functions (and repetition of

this process of all the layers) the output values are calculated. Then, in supervised learning, these output values are compared to the actual values that have been entered into the system by the user beforehand through a cost function. Finally, via the usage of the gradient descent algorithm on the cost function, through the process of backpropagation, the weights and bias values will be changed constantly in an attempt to yield a smaller value of error. The process is terminated when a termination condition is reached. Figure 3.28 displays the network configuration used in MATLAB to compile this model.

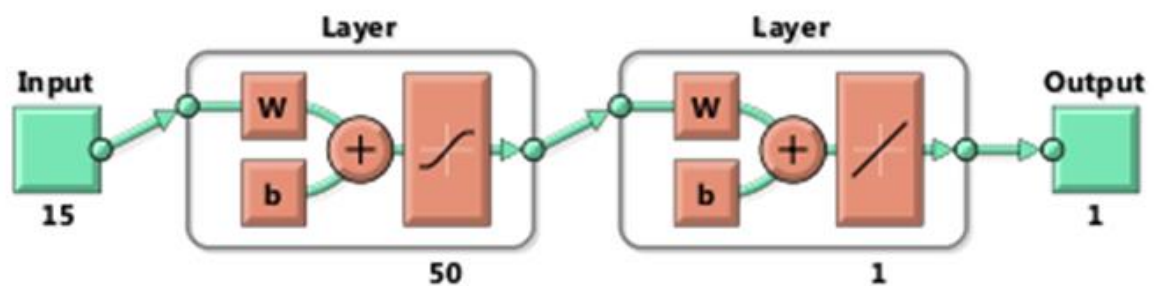


Figure 3.28 Network configuration in MATLAB

Table 3.4 shows in tabular form, the parameters of the network which was used in Method 6. Figure 3.29 shows the result of classification using method 6 where the pixels identified as skin are visible in red.

Table 3.4 Specifications of the trained neural network model (Method 6)

Network Element	Value
Pathway direction	Feed Forward (FF)
Nodes connection type	Fully Connected (FC)
Activation function	Tansig and Purelin
Training function	Traingda (gradient descent, adaptive learning rate)
Cost (performance) function	Mean Squared Error (MSE)
Hidden layer	1 hidden layer
Termination condition	10000 epochs reached
Features	15 selected features
Type of learning	Supervised Learning (SL)



Figure 3.29 Points classified as skin in method 6 (ANN)

Table 3.5 shows in brief the specifications of models used in the six methods.

Table 3.5 Summary of the specifications of the models

Method	Feature type	Selected Bands	Algorithm	
			Name	Descriptions
1	Reflectance	13 bands	SAM	Different thresholds were examined
2	Reflectance	12 bands	SM (Euclidean Distance)	Different thresholds were examined
3	Reflectance	13 bands	SAM	Logical "and" between the results of the two is used
	Reflectance	12 bands	SM (Euclidean Distance)	
4	Reflectance	13 bands	SAM	Logical "and" between the results of the two is used
	Reflectance 1 st Derivative	5 bands	SM (Euclidean Distance)	
5	Reflectance	15 bands	kNN	k=5 has been selected
6	Reflectance	15 bands	FCFF Neural Network	1 hidden layer with 50 nodes, tansig, traingda, traingdx as activation and backpropagation.

3.8. Results of the evaluation

The results (confusion matrices) will be presented in this section in Figure 3.30.

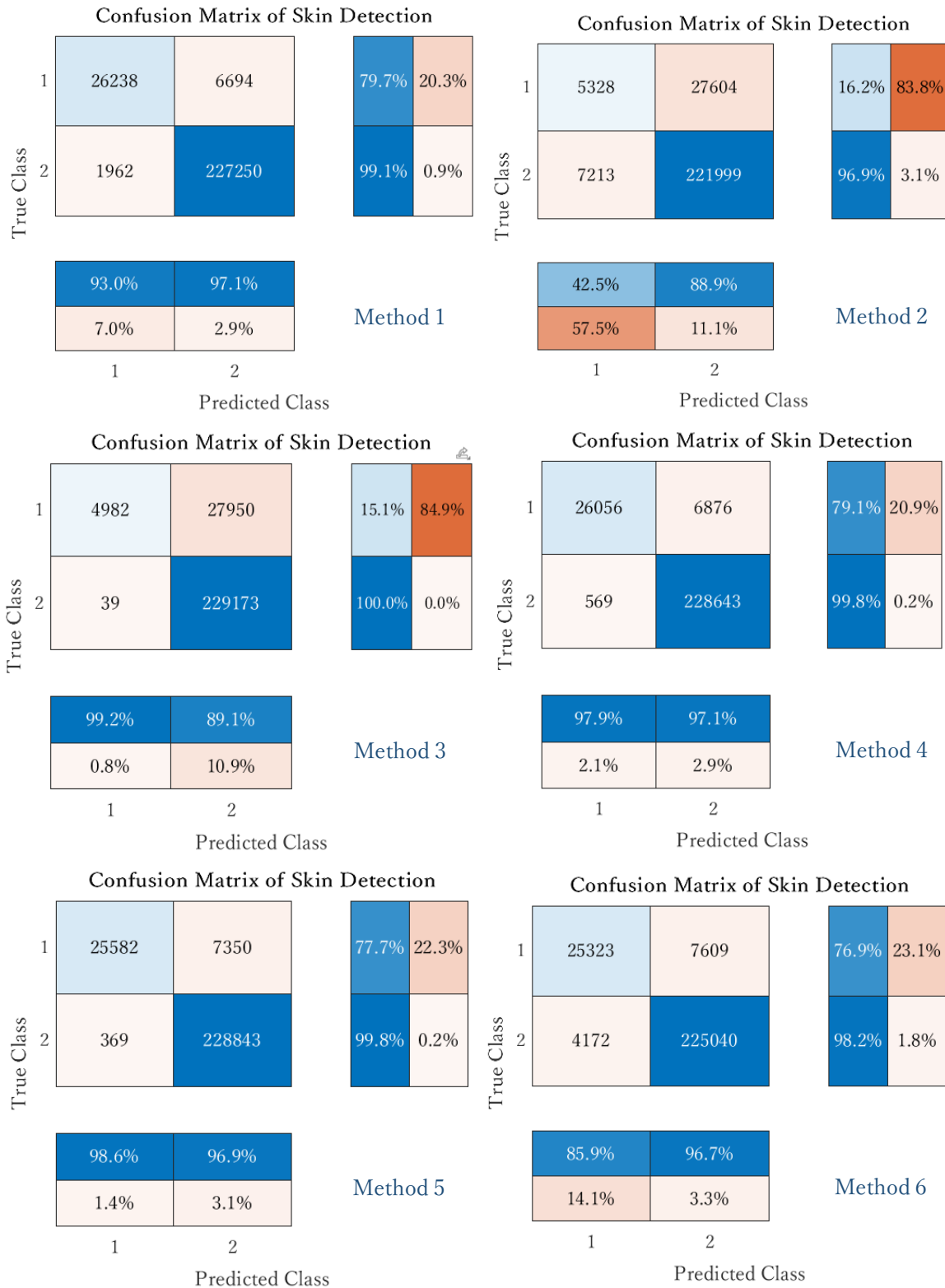


Figure 3.30 Confusion matrices of the classification methods 1 through 6.

As was explained in item 2.2.3, the confusion matrices are used as the fundamental units of evaluation in binary classification problems. From the confusion matrices, values of accuracy, precision, recall and F1 score may be calculated. For each of the methods, the four mentioned metrics are calculated and are available in Table 3.4. It is observed that although Method 2 and Method 3 do not result in a good recall or F1 score value, and the number of detected False Negatives (FN) are very high for these methods, their accuracy is still a large number. This would mean that accuracy is not in itself a suitable measure of evaluation, and other metrics also need to be definitely taken into account.

Although different metrics have different meanings and are beneficial for certain applications, in this study, the final ranking of the models is carried out using accuracy and F1 score. The F1 score is used as a combination of precision and recall, so both are accounted for at the same time. Based on this ranking system, Method 4 is calculated to be the best method, and the next ones are, in order, Method 5, Method 1, Method 6, Method 3 and Method 2.

3.9. Summary of the results

Table 3.6 displays a summary of the evaluation of classification methods.

Table 3.6 The summary of the evaluation results of methods 1 through 6

Method	Algorithm	Accuracy	Precision	Recall	F1 Score
1	SAM (reflectance)	96.6	93.0	79.7	85.8
2	Euclidean distance (reflectance)	86.7	42.5	16.2	23.4
3	SAM (reflectance) + Euclidean distance (reflectance)	89.3	99.2	15.1	26.2
4	SAM (derivative of reflectance) + Euclidean distance (reflectance)	97.1	97.9	79.1	87.5
5	k-Nearest Neighbors (kNN)	97.0	98.6	77.7	86.9
6	Neural network (ANN)	91.2	85.9	76.9	81.1

Figure 3.31 has the collection of all classified images from the previous section.

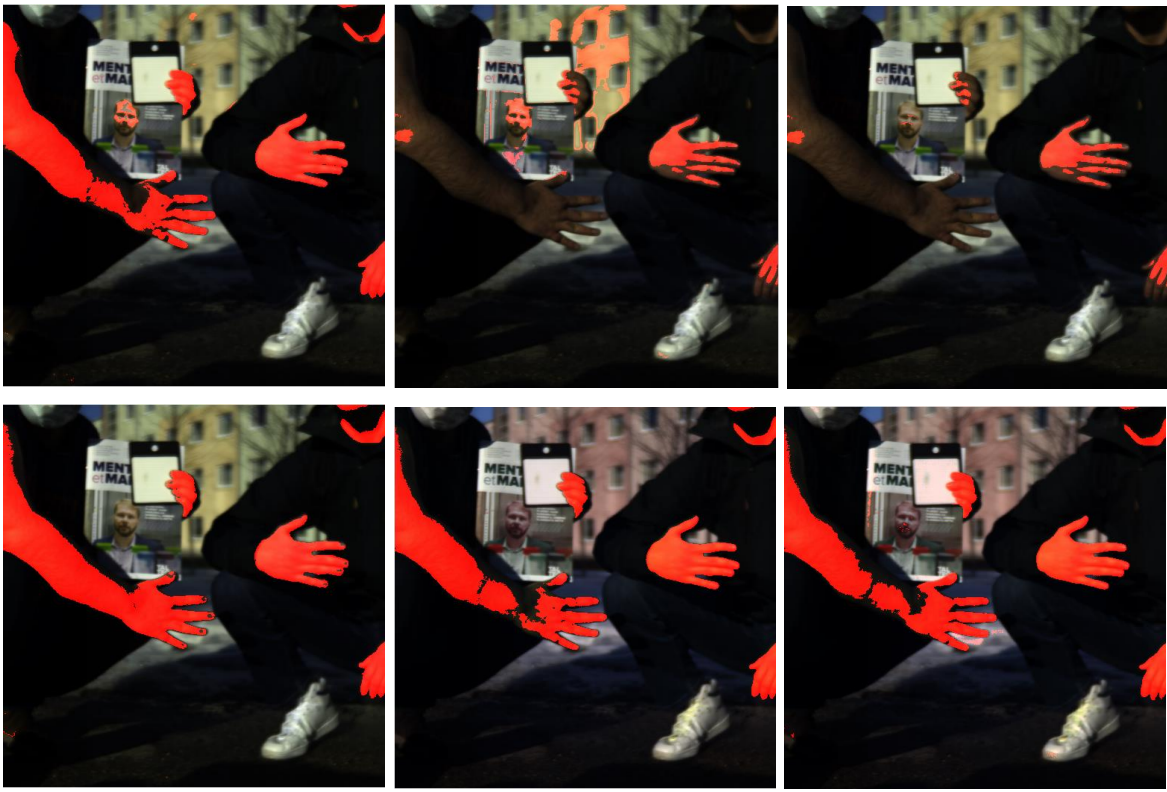


Figure 3.31 The image results of skin classification laid out via the six methods.

4. THE SOFTWARE

To complement the development of the code related to the HS image analysis, and to fill the gap of the availability of a self-explanatory graphical tool for qualitative and quantitative investigation and explore of HS images in MATLAB, a software application was designed with a focus on the needs of the people in engineering and science community, and the needs of the people who are amateur in coding or are learners of HSI technology. In this chapter, a deeper introduction to the software will be carried out.

The code for the software was originally developed in MATLAB and Python, but was continued in Matlab for the better integration options it offered, and in line with the initial goals and the target user group. The layout and the code were developed at the start in the "GUIDE" environment, and were later migrated to "App Designer" environment as GUIDE is going to be decommissioned in the near future. These two environment are part of the MATLAB programming environment offering interactive development possibilities for the design of the interface and programming of the elements and behaviors. [59]

4.1. The interface

The application consists of a main frame (main windows), and a modules frame that is sub-divided into five different tabs (modules) for better usability and simplicity of use. Figure 4.1 displays how the application starts when it is run.

4.1.1. Image display and spectral information

The first four tabs are assigned mainly to display, processing, extracting information of choice, and analysis of the image. In case of need, the user can save the resulting image and various possible graphs (including the material spectral signature graph).

Under the "Display" tab, the image may be loaded and the fingerprint (spectral signature) for each pixel can be graphed. The fingerprint of an HSI pixel (P) consists of ordered pairs of the reflectance values (as a function of wavelength or band number), and their corresponding wavelengths (or bands) at point P , registered by the camera. Equations (2.1) and (2.2) represent a formulated version of what the fingerprint is.

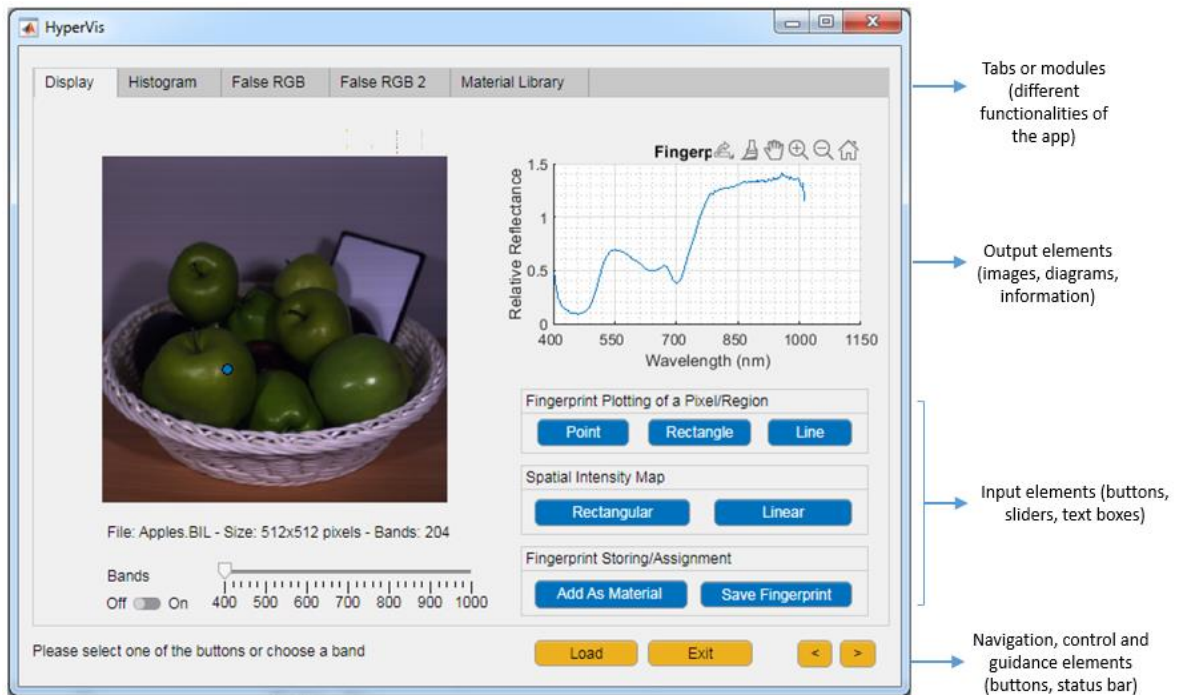


Figure 4.1 "Display" tab of the interface. This tab is the active tab when the application starts.

Based on the choice of the user, in the panel "Fingerprint Plotting of a pixel/region", the fingerprint diagram of one or more pixels may be displayed. It is also possible for the user to view the spatial intensity map of a set of pixels at a specific band. The intensity map at a certain band previews a map in which in place of each pixel sits its intensity value at that specific band. In short, a fingerprint describes the behavior of a pixel through all bands, and an intensity map is representative of the behavior of all pixels in one band. It is also possible to view the picture in each band. The fingerprint and the intensity map are depicted in Figures 1 and 2 respectively.

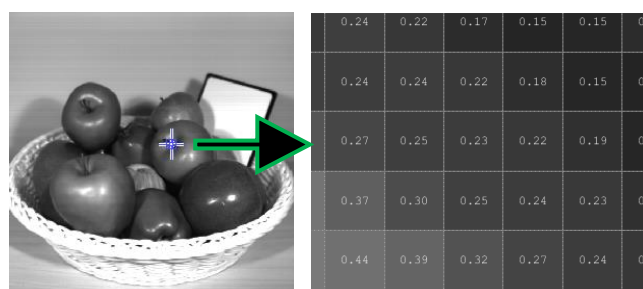


Figure 4.2 Spatial intensity map (right) at a certain region marked on the image (left)

The "Add as Material" button stores the selected pixel's fingerprint as a new material, and in this way, the user may store a set of materials, based on which they can further

classify materials in images, or use those materials for a comparative study of similarities and dissimilarities.

4.1.2. Image histograms

Under the tab named "Histogram" (Figure 4.3), after the selection of a specific band (or wavelength) by the slider, the corresponding image of that band is shown together with the histogram and the cumulative histogram at that band. In the next step, the equalized histogram of the band is displayed (bottom right diagram), and the equalization is applied to the original image at the specified channel. Being able to view the images and the graphs side by side, and immediately examining the effect of the equalization process on every channel of an image can be useful in situations where the image suffers from inappropriate contrast leading to some elements not being clearly detectable. An instance of such an occurrence is when proper lighting is not present, or when pixels are too bright.

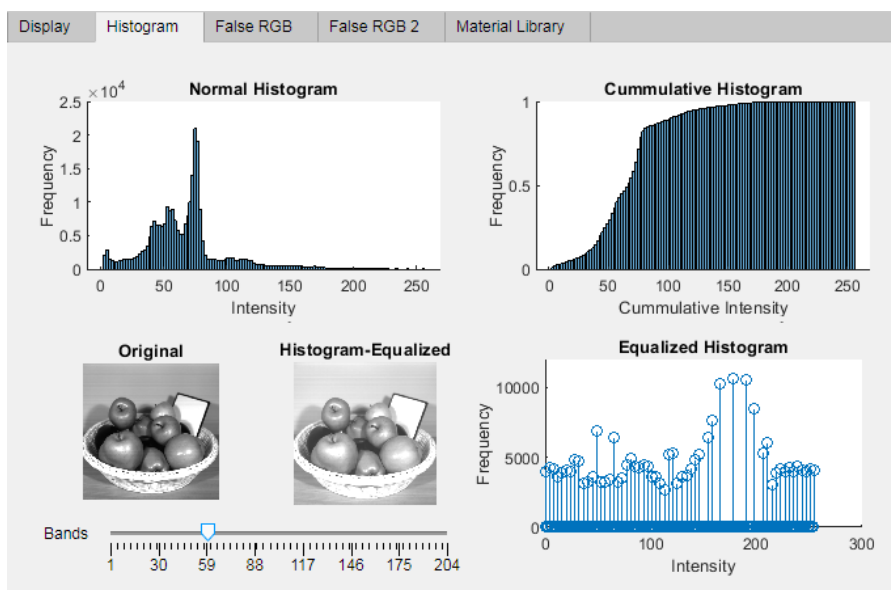


Figure 4.3 "Histogram" tab, including three types of histograms and their corresponding images

4.1.3. False RGB image

By selecting of 3 bands and assigning them to primary RGB (Red, Green, Blue) colors, it is possible to view the effects of channel combination on the image. This can be beneficial in gaining an understanding of the HS data in relation to the primary RGB data that is comprehended by the human visual system, for purposes such as qualitative analysis, lighting evaluation, object detection, feature extraction, image correction, etc.

The tab titled "False RGB" is meant for carrying out the mentioned selection and display. Figure 4.4 shows three images produced by this tab. Each image depicts a different combination of bands (i.e., different merged image).

For each point P , the set of all possible combinations of 3 bands (S_3^P), is the set of all ordered triplets like $(R^P(i), R^P(j), R^P(k))$ whose members are band reflectance values at point P (Equation (4.1)). The members of such triplets are not required to be unique, i.e., $R^P(i)$ can have the same value as $R^P(j)$ or $R^P(k)$.

$$S_3^P = \{(R^P(i), R^P(j), R^P(k)) \mid i, j, k \in \{1, \dots, N_b\}\} \quad (4.1)$$

Where $R^P(i)$ is the reflectance value of point P at band i , and N_b is the total number of bands registered by the camera. If reflectance values for three specific bands are considered for every pixel in the image, and these reflectance intensity values of each band are merged in the end, the result is going to be a merged image of those three bands. Each unique selection of the triplets maps to a unique merged image. In an image with N_b bands, the number of possible combinations of three bands is $N_b \times N_b \times N_b$. For the specific 204-band sample image that we used, such combinations will add up to $204^3 = 8489664$ combinations (i.e. 8489664 possible three-band merged images).

The image in Figure 4.4 (a) is formed by opting for band 70 to be interpreted as the red channel, band 53 to be interpreted as the green channel, and band 19 to be interpreted as the blue channel. The respective wavelengths for these bands in SPECIM IQ camera are $\lambda_R = 449.35$ nm, $\lambda_G = 548.55$ nm and $\lambda_B = 598.60$ nm. This image (Figure 4.4 (a)) is the closest image to what is visible by the human eyes, hence it is known as the "true" RGB image. All other combinations, such as the ones present in Figure 4.4 (b) and Figure 4.4 (c) are known as the "false" RGB (fRGB) images in HSI terminology.

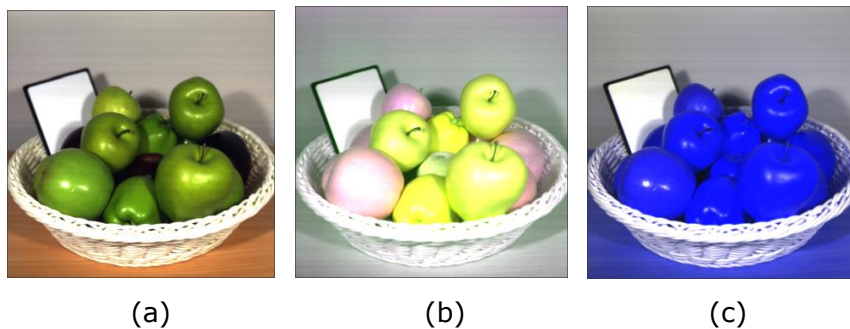


Figure 4.4 The true RGB image (a), and two false RGB images (b) and (c)

The "False RGB 2" tab serves the user with more information about the three selected channels discussed in previous paragraphs. In this tab, the histograms of the three channels are separately displayed. Also, the pie chart of the ratio of the cumulated value of the selected bands is calculated for better investigation of the image. For both tabs "False RGB" and "False RGB 2", the selection of the bands is conducted by the three sliders in the right half of the tab and under "Wavelength/Band Selection for R, G, and B" panel, or through their adjacent text boxes.

It is also possible to conduct point operations on the image. Multiplication, addition (shifting), and/or a combination of them may be applied to images. Point operation is a mapping of values of intensity of a channel in an image in which the new intensity value of a pixel depends only on its previous intensity value. If we denote this transformation with $f()$, the input image with $I(u, v)$, and the resultant image with $J(u, v)$, and l_1 and l_2 are image width and height respectively, we can write Equation (4.2):

$$f(I(u, v)) = J(u, v) \quad u \in [0, l_1], v \in [0, l_2] \quad (4.2)$$

For the two named operations (addition and multiplication), the image pixels are mapped according to the following relation:

$$f(I(u, v), C_1, C_2) = C_1 \times I(u, v) + C_2 \quad (4.3)$$

In Equation (4.3), $C_1 \in \mathbb{R}$ is a constant value identified by the user which is multiplied by all the intensity values of pixels of the image channels (R, G and B), and "×" symbol represents the multiplication of a matrix by a constant value. In a similar fashion, $C_2 \in \mathbb{R}$ is a constant value identified by the user that is added to each of the intensity values of pixels of image channels.

Under "Intensity Shifting or Multiplication" panel, it is possible to change the value of C_1 and/or C_2 . As explained, this value is going to be multiplied by or be added to each of the selected channels' (R, G or B) intensity values. The user may choose which of the values (C_1 or C_2) should change by selecting "Shift" or "Multiply" (Figure 4.5). For instance, if the value selected by the vertical "G" lever (slider) is $E_G = 0.5$ and the operation to be done is set to "Multiply", all intensity values in the green channel will be multiplied by $C_1 = 10^{E_G} = 3.16$. If I_G is the matrix of intensity values of pixels in the green channel, this operation can be presented by $I_G \times 10^{E_G}$. The default value for C_1 is 1 and for C_2 is 0. Since the intensity values are positive or zero, positive values for C_2 shift the

histogram to the right, and negative values shift the histogram to the left. For $C_1 > 1$ an increase in the intensity values happen, and for $0 < C_1 < 1$, those values undergo a decrease. In turn, this may cause the histogram of a band to stretch or shrink [60]. Also, the user can choose to save the configuration or save the false RGB image.

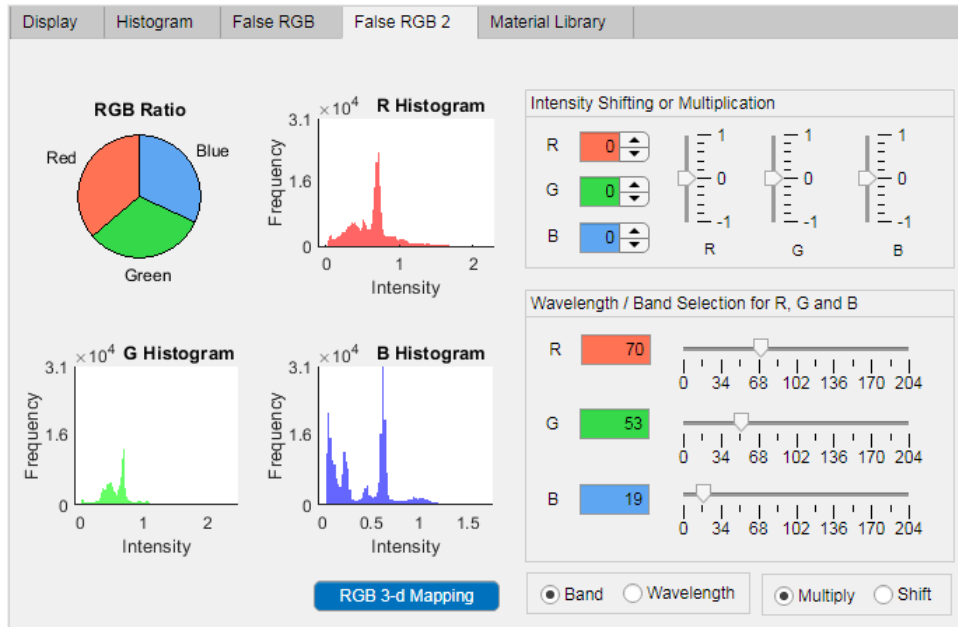


Figure 4.5 "False RGB 2" tab. Reflectance intensity histograms and RGB ratio pie chart of the three bands

4.1.4. Data handling

Concerning the input data, one must ensure interoperability between different formats of HS images. Towards this end, the current version of the developed application supports the most popular structures, namely "BIL", "BSQ", and "BIP" [61]

4.2. Case study

As a major application in Mechatronics and Robotics, engineers deal with pick and place algorithms which may consequently require material/color detection.

One of the challenges faced in picking operations is to recognize/detect two objects/materials with closely-identical color and appearance (for later sorting). With RGB images, this may not be feasible in specific cases, but with hyperspectral images, such cases may be resolved with much more accuracy. As can be seen in Figure 4.6, although the two marked apples ("Apple 1" and "Apple 2") are visually very similar to

each other in Figure 4.6 (a), with the proper selection of the bands, the distinction can be made with a high level of confidence (as shown in Figure 4.6 (b)), offering much higher accuracy in comparison with a true RGB image.

In order to better demonstrate how our proposed software can be beneficial in certain applications, in this section, an approach to perform this task with the usage of our software tool is elaborated on. Hence, we intend to be able to distinguish between the two numbered apples marked in Figure 4.6 (a), and expose the investigated difference visually, solely using our software. The multi-step procedure is as follows.

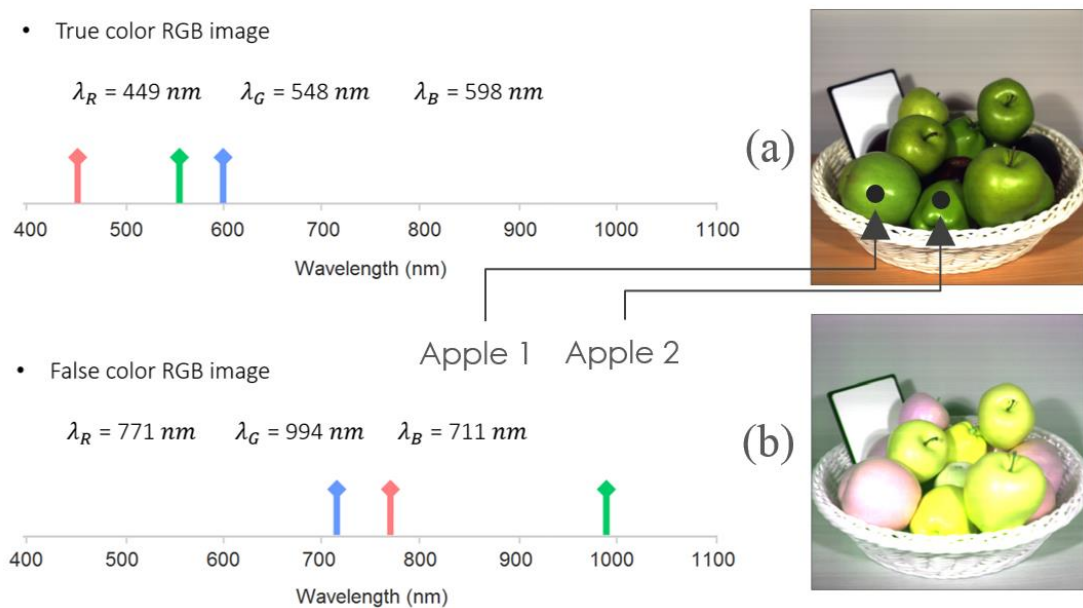


Figure 4.6 The true RGB image (a), and the generated False RGB image where the annotated apples are clearly distinguishable (b). On the left, the corresponding wavelengths that are interpreted as R, G and B bands can be found.

4.2.1. Looking for the differences

After loading the image, properties of the two apples under focus are to be investigated. This investigation is conducted with the goal of finding differences that may help in distinguishing the apples. We take the fingerprints of two arbitrary pixels on the two marked apples (Figure 4.6) by selecting one of their pixels in the "Display" tab using "Fingerprint Plotting" point tool. Then, these two fingerprints are compared (Figure 4.7), and although they appear closely similar, there are a number of bands (wavelengths) at each of which an obvious intensity difference can be observed. We locate the approximate wavelength of three of such bands as shown by arrows in Figure 4.7.

The three bands that were detected (with approximate wavelengths of $\lambda=710$ nm, $\lambda=770$ nm, $\lambda=990$ nm) have the potential to reveal the difference between the two apples, and thus will be used to carry out the next step.

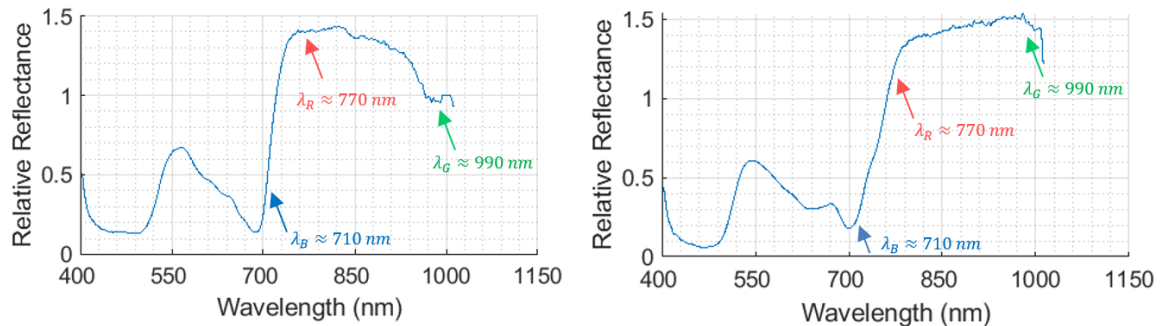


Figure 4.7 The fingerprint of a pixel on “Apple 1” (left), and on “Apple 2” (right). The three arrows show at what wavelengths the largest differences exist between the two apples’ fingerprints

4.2.2. Exposing the differences

To visually exhibit the effect of the selection of the found channels (wavelengths) to compose an RGB image, we choose the three bands to be interpreted as R, G and B values in the “False RGB” tab under “Wavelength/Band Selection” panel. After examining different values for different arrangements of R, G and B, a false RGB image is produced in which the two apples (“Apple 1” and “Apple 2” in Figure 4.6) are distinctively viewable, and their hidden difference is now visually revealed.

The resulting image is present in Figure 4.6 (b). The final combination of the wavelengths (bands) for this task is $\lambda_B = 771$ nm, $\lambda_G = 994$ nm, and $\lambda_R = 711$ nm. As it can be observed, the result is highly accurate in making a distinction between the two apples.

4.2.3. Further processing

Alongside the steps taken to perform the analysis, it is possible through the “Histogram” tab and “False RGB 2” tab to analyze the image and its properties further and do processing tasks (like some linear point operation or histogram equalization) on the image.

4.2.4. The usage flow to perform the task

The flow of the actions that were considered for finding the distinction between the two apples can be visualized with the help of a chart in which operations, results, and sequence of actions are depicted. For our specific case, Figure 4.8 shows one of the ways that the sequence of the taken actions, and other optional possible actions may be laid out.

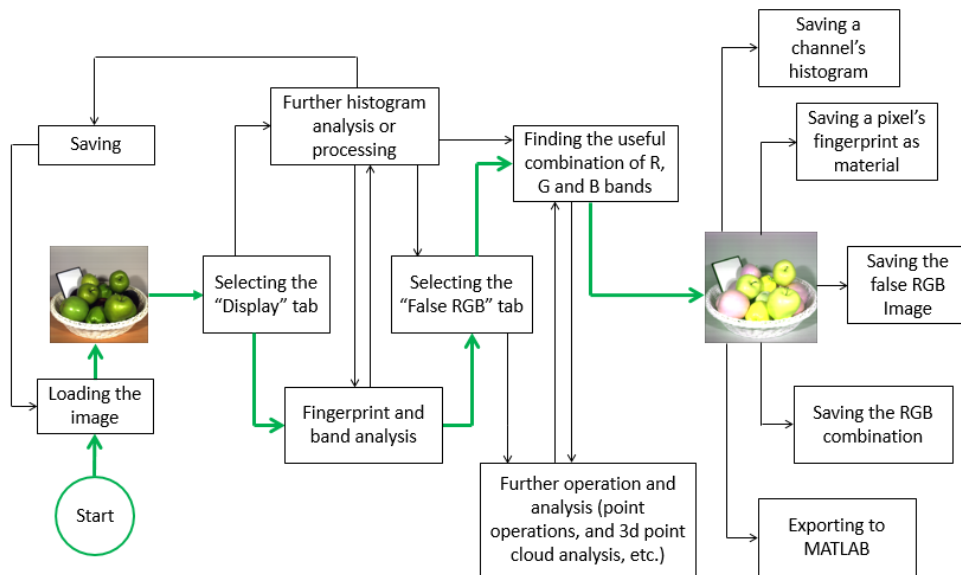


Figure 4.8 Flow of the actions taken to detect the difference between the two apples

in Figure 4.8, and to reveal this difference in a visually observable manner, using the current proposed software. The path that was taken to perform this specific task (finding a clear distinction between the two apples) is displayed in green color, and the path for other possible operations (options) is visible in black. Each rectangle represents an action that is possible throughout the flow. The outflow of each step is identified by an outgoing arrow which connects an action (or the result of an action) to the next possible actions (rectangles).

This specific application is one of the tasks that are possible through our software application enabling the user to perform image analysis. There are also other paths to perform the same task with the software, and the stated sequence of actions in this section is only one of them. As explained, such analysis can be taken even further through the other sections and other functionalities of the proposed software.

4.2.5. Summary of the specifications

In Table 4.1, a summary of the application’s specifications are provided.

Table 4.1 GUI application specifications

Group	Sub-group	Items	Item Details
Development Environment	Development environment/language	MATLAB	Versions 2019b and 2021b
	GUI Development environment	App Designer	In-built MATLAB tool
Dependencies	Needed Libraries (add-ons)	Signal Processing Toolbox Image Processing Toolbox Deep Learning Toolbox Computer Vision Toolbox	Only MATLAB native libraries are needed
Visual Elements	Input Elements	textbox, slider, button, etc.	
	Output Elements	axis (graphs and images), text, label	
	Navigation Elements	button, status bar (text box), tabs, panels	
Operating System	The OS used for development	Windows	Versions 7, and 10
A hardware configuration that works	Processor, Memory, Disk Space	1-2 GB of RAM (dedicated to app), core i7, 100 MB of disk space is recommended	

5. DISCUSSION AND FINAL REMARKS

5.1. Methods performance

For the purposes of this research, selection of a ranking system for the evaluation of the final results was discussed in section 3.8 and based on the data collected in Table 3.6, further investigation can be performed. Overall, the best method regarding the accuracy and F1 score is Method 4, where accuracy is 97.1 % and the F1 score is 87.5 %. This method has an acceptable performance regarding recall and precision too. Method 5 (kNN) and Method 1 (SAM) proved to be the next best methods with the same two criteria, respectively. Although the value of recall is larger in Method 1 (than the two named methods), the small difference of 0.6 % and 2.0 % may be neglected. The neural network method (Method 6) is also not performing weakly, but the performance is weaker than the other three methods and is very sensitive to the training set. This high sensitivity is a fact that we expected and matches the findings in [62]. So, Method 6 is ranked 4th regarding both F1 score and accuracy. Method 3 and Method 2 exhibit very small recall values corresponding to the very small F1 score turning them to weakest methods out of the 6 studied methods. The high precision value in Method 3 is then not considered a significant advantage for this method. Figure 5.1 is expressive of the discussed results.

The proposed addition of 1st spectral derivative as a feature, which was performed in Method 4, helps in reducing FP points such as the fake skin, but has not any effect on FN points. It accords with our expectations, as the addition of a condition through a “logical and” may only reduce the false positives. All considered, it might be said that the proposed addition has improved the results gained by this method inserting it in the first place when the overall performance is considered. For further improvement of method 4, usage of the 2nd spectral derivative is recommended.

Lighting is important in general in all the methods. It seems that methods based on Euclidean distance suffer very much from insufficient lighting and methods based on angular distance are resistant toward lighting changes. This fact is also in line with findings in [38].

Regarding the speed of running the methods, ANN is the slowest both in training and in prediction and SAM is the quickest method. Generally, methods based on spectral matching are fast methods and may be considered when speed is a critical concern.

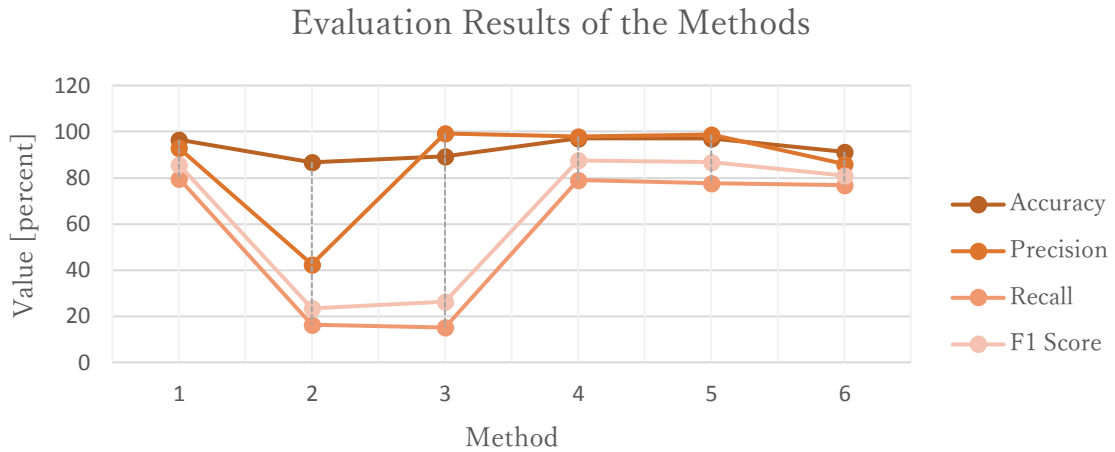


Figure 5.1 The four evaluation measures of the methods used

5.2. Software

The development of the software with the planned specifications was achieved as the third main goal of this research. It was demonstrated that the various components of the application used together allow for the analysis and processing of an input image so that the user could extract qualitative and quantitative information and use them for further operations, such as material classification. The user does not have to have extensive knowledge of computer-related fields or bold domain knowledge in digital imaging to be able to use the application. Finally, the application was developed so that the composition and arrangement of the interface are geared towards understandability, simplicity and having meaningful relationships with theoretical/academic concepts, making it suitable to be utilized for educational purposes.

5.3. Applications

By making use of the computer learning and spectral processing methods, two cases of material classification/detection were studied in elaboration in chapters 3 and 4. Such applications may be further consumed as part of a bigger system or algorithm such as pick-and-place algorithm, or the detections systems in an autonomous car.

It should be noted that the evaluation of a method needs to account for the specific application that is intended for that method. For instance, for the detection or classification of human skin for rescue operations or in autonomous cars, it is very

important that the model outcomes the minimum amount of missed human skin pixels. So the number of false-negative results should strictly be kept at a minimum and hence “recall” will be the most influential measure among all the evaluation metrics.

The type of the application, and the subject under study, may also introduce restrictions/instructions for the selection of the best features. This may also be affected by the specific domain knowledge. For instance, for the classification of apples, domain knowledge of food sciences may come into play.

Mixed usage of sensors (sensor fusion) with hyperspectral imaging sensors can also influence the overall process of classification, and is recommended in many of the applications.

5.4. Verifying that the initial goals are met

According to what was mentioned in previous sections of this chapter, it is possible to claim that the initial goals has been met in line with our expectations.

5.5. Future work

Many areas for future work may be considered. Some topics are as follows:

- Consideration of optimized imaging parameters (like lighting) when acquiring the images. It may consist of using helping devices such as lighting softboxes.
- Expanding the dataset to include larger amount of instances through choosing a larger number of imaging subjects, larger number of lighting conditions, etc.
- Usage of different mixtures of features, engineered feature and similarity measures. Specifically, using the second derivative of reflectance values may help in the classification process.
- Incorporation of different computer learning methods, and optimization of their parameters using techniques such as grid search
- Considering the software development in programming languages with better capabilities for memory management, or faster languages for image processing like the programming language C.

5.6. Schematic summary of the operations and data flow

The following figure provides a summarized presentation of the operational flow discussed in chapters 3 and 4 and concluded in the current chapter.

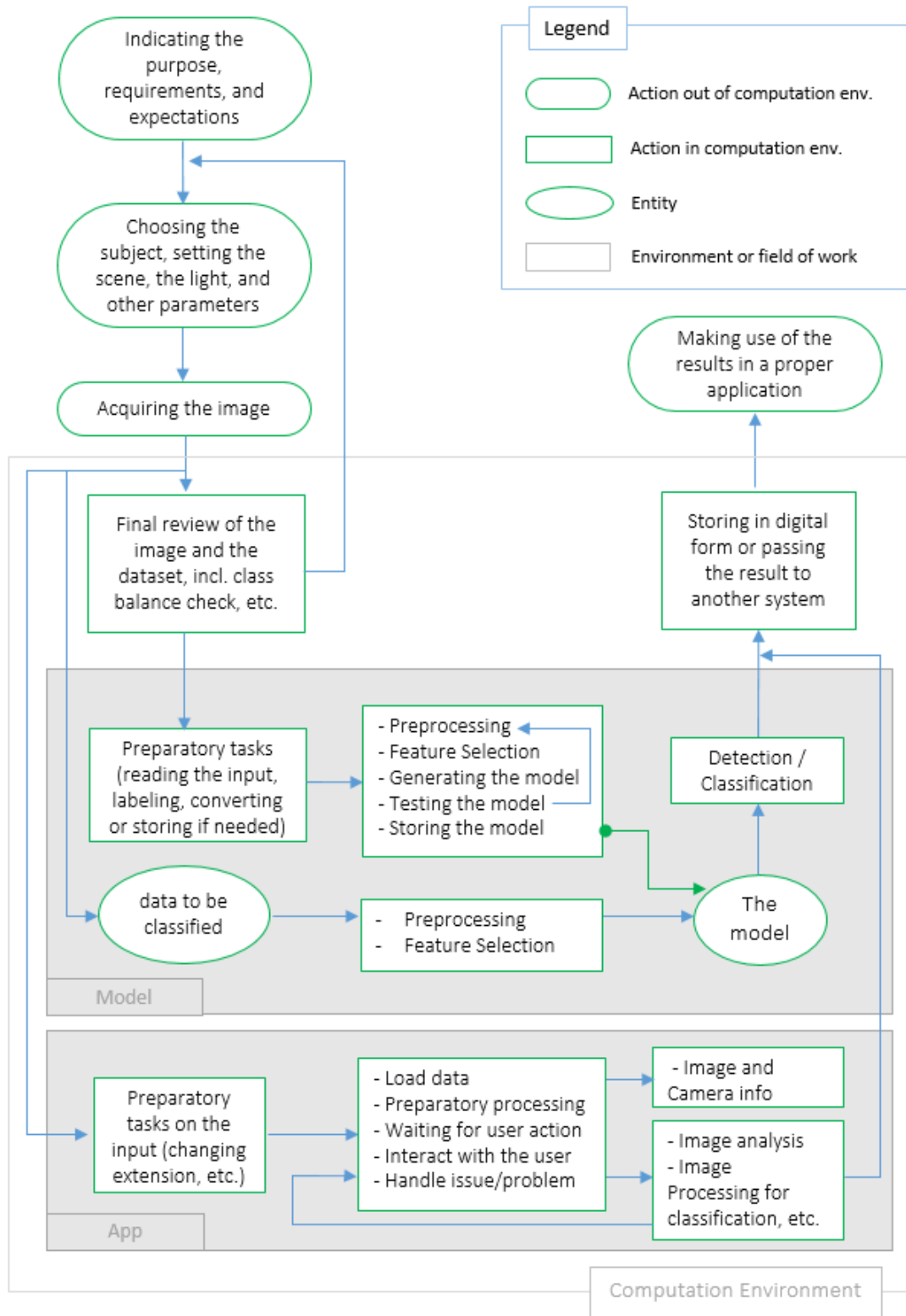


Figure 5.2 Schematic summary of the operations and data flow in the scope of this thesis work

6. SUMMARY

The intent of this work was to investigate how computational methods may be useful in the analysis and classification of hyperspectral imaging data, and to further facilitate the processing of hyperspectral images for a wider range of users, a MATLAB Graphical User Interface (GUI) application was developed. For this to come true, hyperspectral computer vision, data processing, machine learning algorithms, GUI application programming and their related areas needed to be brought under focus and study.

The initial phase is compiling the models and applying them to hyperspectral data. This begins with acquiring of the images incorporating hyperspectral imaging techniques. Then the dataset is formed, reviewed and moves to a 5-step preprocessing pipeline. Two options for feature selection are considered, with one focusing on the local extrema of spectral signatures and the other on the variance of the features. At this step, the six compiled models are adapted to the problem and are executed. Finally, the methods are tested using evaluation measures of binary classifiers. The best method regarding the accuracy and F1 score is Method 4 with an accuracy of 97.1 and F1 score of 87.5. Method 5 (kNN) and Method 1 (SAM) are next with F1 scores of 86.9 and 85.8 respectively. The precision of Method 3 was the highest among all being 99.2 but it has a poor performance regarding the overall F1 score. Method 6 (ANN) shows a high sensitivity to the training data, while SAM-based methods proved to be less influenced by illumination. Speed-wise, Methods 1 and 2 have overcome other methods.

Alongside compiling the methods, the second concern of the research was addressed by proposing specific usage of spectral derivatives as a feature (in Method 4). It improved the F1 score of method 1 by 1.66 and was chosen as the best method overall.

Thirdly, as a complement to the developed procedures, to provide a graphical user interface for the analysis and processing of hyperspectral images, a software application in MATLAB was laid out and programmed. Target groups in the scientific community, academia, and practitioners who are not familiar with coding may benefit from such software tool. With a self-explanatory interface, this application has the potential to be used for educational purposes too. This contribution has also been presented at an international conference in June 2021 [63].

It may consequently be claimed that the three initial concerns which led to conducting this research work have been addressed and the three research questions are answered.

KOKKUVÕTE

Käesoleva töö eesmärk oli uurida, kuidas arvutusmeetodid võivad olla kasulikud hüperspektraalsete kujutiste andmete analüüsimisel ja klassifitseerimisel ning hõlbustamaks veelgi hüperspektraalsete kujutiste töötlemist laiema kasutajatehulga jaoks töötati välja MATLAB graafilise kasutajaliidese (MATLAB Graphical User Interface - GUI) rakendus. Et see teoks saaks, tuli fookusesse tuua ja uurida hüperspektraalset arvutinägemist, andmetöötlust, masinõppe algoritme, GUI rakenduste programmeerimist ja nendega seotud valdkondi.

Algaasiks on mudelite koostamine ja nende rakendamine hüperspektraalsetele andmetele. See algab hüperspektraalseid pilditehnikaid sisaldavate kujutiste hankimisega. Seejärel moodustatakse andmestik, vaadatakse see üle ja liigutakse 5-astmelisele eeltöötluskonveierile. Kaalutakse kahte funktsiooni valikuvõimalust, millest üks keskendub spektraalsignatuuride lokaalsele ekstreemumile ja teine tunnuste dispersioonile. Selles etapis kohandatakse kuus koostatud mudelit probleemi jaoks ja rakendatakse need. Lõpuks testitakse meetodeid binaarsete klassifikaatorite hindamismeetmete abil. Parim meetod täpsuse ja F1 skoori osas on meetod 4 täpsusega 97,1 ja F1 skooriga 87,5. Meetod 5 (kNN) ja meetod 1 (SAM) on järgmised F1 skooridega vastavalt 86,9 ja 85,8. Meetodi 3 täpsus 99,2 oli kõigist kõrgeim, kuid meetodi tulemus on F1 üldise skoori osas kehv. Meetod 6 (ANN) näitab koolitusandmete suhtes suurt tundlikkust, samas kui SAM-põhised meetodid osutusid valgustusest vähem mõjutatuks. Kiiruse osas ületavad meetodid 1 ja 2 muid meetodeid.

Meetodite koostamise kõrval käsitleti uurimistöö teist eesmärki, pakkudes tunnusena välja spektraalderivaatide spetsiifilise kasutamise (meetodis 4). See parandas meetod 1 F1 skoori 1,66 võrra ja valiti üldiselt parimaks meetodiks.

Kolmandaks, väljatöötatud protseduuride täiendusena, pakkumaks hüperspektraalsete kujutiste analüüsiks ja töötlemiseks graafilist kasutajaliidest, koostati ja programmeeriti MATLAB-i tarkvararakendus. Sellisest rakendusest võivad kasu saada sihtrühmad teadusringkondades ja akadeemilistes ringkondades, samuti praktikud, kes ei tunne kodeerimist. Lihtsalt arusaadava liidesega on seda rakendust võimalik kasutada hariduslikel eesmärkidel. Töö sisu ja tulemusi on tutvustatud rahvusvahelise konverentsi ettekandes 2021.a. juunis [63].

Sellest tulenevalt võib väita, et kolm esialgset eesmärki, mis viisid selle uurimistöö läbiviimiseni on lahendatud ja kolm uurimisküsimust on saanud vastuse.

REFERENCES

- [1] W. Salah Alaloul and A. Hannan Qureshi, "Material Classification via Machine Learning Techniques: Construction Projects Progress Monitoring," in *Artificial Neural Networks and Deep Learning - Applications and Perspective*, IntechOpen, 2021.
- [2] N. C. Basantia, L. M. L. Nollet, and M. Kamruzzaman, *Hyperspectral imaging analysis and applications for food quality*. 2018.
- [3] A. Schneider and H. Feussner, "Diagnostic Procedures," in *Biomedical Engineering in Gastrointestinal Surgery*, Academic Press, 2017, pp. 87–220.
- [4] L. Prangnell, "Visible Light-Based Human Visual System Conceptual Model," Sep. 2016, doi: 10.48550/arxiv.1609.04830.
- [5] A. Lowe, N. Harrison, and A. P. French, "Hyperspectral image analysis techniques for the detection and classification of the early onset of plant disease and stress," *Plant Methods*, vol. 13, no. 1, Oct. 2017, doi: 10.1186/S13007-017-0233-Z.
- [6] C. H. Bock, J. G. A. Barbedo, E. M. Del Ponte, D. Bohnenkamp, and A.-K. Mahlein, "From visual estimates to fully automated sensor-based measurements of plant disease severity: status and challenges for improving accuracy," *Phytopathol. Res.*, 2020, doi: 10.1186/s42483-020-00049-8.
- [7] G. ElMasry and D. W. Sun, "Meat Quality Assessment Using a Hyperspectral Imaging System," *Hyperspectral Imaging Food Qual. Anal. Control*, pp. 175–240, 2010, doi: 10.1016/B978-0-12-374753-2.10006-1.
- [8] B. Fei, "Hyperspectral imaging in medical applications," in *Data Handling in Science and Technology*, vol. 32, Elsevier, 2019, pp. 523–565.
- [9] M. R. Resende, L. L. B. Bernucci, and J. A. Quintanilha, "Monitoring the condition of roads pavement surfaces: proposal of methodology using hyperspectral images," *J. Transp. Lit.*, vol. 8, no. 2, pp. 201–220, Apr. 2014, doi: 10.1590/S2238-10312014000200009.
- [10] M. B. Stuart, A. J. S. McGonigle, and J. R. Willmott, "Hyperspectral Imaging in Environmental Monitoring: A Review of Recent Developments and Technological Advances in Compact Field Deployable Systems," *Sensors 2019, Vol. 19, Page 3071*, vol. 19, no. 14, p. 3071, Jul. 2019, doi: 10.3390/S19143071.
- [11] J. Behmann *et al.*, "Specim IQ: Evaluation of a New, Miniaturized Handheld Hyperspectral Camera and Its Application for Plant Phenotyping and Disease Detection," *Sensors (Basel)*, vol. 18, no. 2, Feb. 2018, doi: 10.3390/S18020441.
- [12] "Resonon Pika XC2 Hyperspectral Imaging Camera." [Online]. Available: <https://resonon.com/Pika-XC2>. [Accessed: 07-May-2022].
- [13] J. Ewing, T. Oommen, P. Jayakumar, and R. Alger, "Utilizing Hyperspectral

- Remote Sensing for Soil Gradation," *Remote Sens.* 2020, Vol. 12, Page 3312, vol. 12, no. 20, p. 3312, Oct. 2020, doi: 10.3390/RS12203312.
- [14] "Specim IQ Data Sheet." [Online]. Available: https://www.specim.fi/downloads/iq/Specim-IQ-Datasheet-Long-05-Web.pdf?vgo_ee=Yr5NWMn8QxsxUk0QtFNKEYvy7T5YEJ8ohjC9vauJg30%3D. [Accessed: 08-May-2022].
- [15] "Illumination - Specim IQ Manual." [Online]. Available: <https://www.specim.fi/downloads/iq/manual/software/iq/topics/illumination.html>. [Accessed: 07-May-2022].
- [16] R. Alamús, F. Pérez, L. Pipia, and J. Corbera, "Urban Sustainable Ecosystems Assessment through Airborne Earth Observation: Lessons Learned ," 2018, doi: 10.5194/isprs-archives-XLII-1-5-2018.
- [17] D. Manea and M. A. Calin, "Hyperspectral imaging in different light conditions," *Imaging Sci. J.*, vol. 63, no. 4, pp. 214–219, 2015, doi: 10.1179/1743131X15Y.0000000001.
- [18] "Calculating the Emission Spectra from Common Light Sources | COMSOL." [Online]. Available: <https://www.comsol.fr/blogs/calculating-the-emission-spectra-from-common-light-sources/>. [Accessed: 07-May-2022].
- [19] S. Schiefer, P. Hostert, and A. Damm, "ANALYSIS OF VIEW-ANGLE EFFECTS IN HYPERSPECTRAL DATA OF URBAN AREAS."
- [20] C. Ruffin and R. L. King, "The analysis of hyperspectral data using Savitzky-Golay filtering-theoretical basis," in *Geoscience and Remote Sensing Symposium, 1999. IGARSS '99 Proceedings. IEEE 1999 International Volume: 2*, 1999, doi: 10.1109/IGARSS.1999.774430.
- [21] H. Huang, L. Liu, and M. O. Ngadi, "Recent Developments in Hyperspectral Imaging for Assessment of Food Quality and Safety," *Sensors 2014, Vol. 14, Pages 7248-7276*, vol. 14, no. 4, pp. 7248–7276, Apr. 2014, doi: 10.3390/S140407248.
- [22] P. Tatzert, M. Wolf, and T. Panner, "Industrial application for inline material sorting using hyperspectral imaging in the NIR range," *Real-Time Imaging*, vol. 11, no. 2, pp. 99–107, Apr. 2005, doi: 10.1016/J.RTI.2005.04.003.
- [23] A. F. H. Goetz, "Three decades of hyperspectral remote sensing of the Earth: A personal view," *Remote Sens. Environ.*, vol. 113, no. SUPPL. 1, Sep. 2009, doi: 10.1016/J.RSE.2007.12.014.
- [24] S. Selci, "The Future of Hyperspectral Imaging," *J. Imaging 2019, Vol. 5, Page 84*, vol. 5, no. 11, p. 84, Oct. 2019, doi: 10.3390/JIMAGING5110084.
- [25] Y. Lu, W. Saeys, M. Kim, Y. Peng, and R. Lu, "Hyperspectral imaging technology for quality and safety evaluation of horticultural products: A review and

- celebration of the past 20-year progress," *Postharvest Biol. Technol.*, vol. 170, Dec. 2020, doi: 10.1016/J.POSTHARVBIO.2020.111318.
- [26] C. C. Cooksey, B. K. Tsai, and D. W. Allen, "A collection and statistical analysis of skin reflectance signatures for inherent variability over the 250 nm to 2500 nm spectral range," 2014, doi: 10.1117/12.2053604.
- [27] S. M. Sanchez and M. Velez-Reyes, "Skin detection in hyperspectral images," *Algorithms Technol. Multispectral, Hyperspectral, Ultraspectral Imag. XXI*, vol. 9472, p. 94721P, May 2015, doi: 10.1117/12.2179332.
- [28] G. G. N. Geweid, F. Vasefi, and K. Tavakolian, "A Novel Nonparametric Technique for Segmenting Multimode Hyperspectral Images Obtained From Non-Melanoma Skin Cancer Lesions," *Front. Biomed. Devices, BIOMED - 2020 Des. Med. Devices Conf. DMD 2020*, Jul. 2020, doi: 10.1115/DMD2020-9045.
- [29] "Benefits of Hyperspectral Imaging for Food Quality Assurance." [Online]. Available: <https://www.advian.fi/en/blog/benefits-of-hyperspectral-imaging-for-food-quality-assurance>. [Accessed: 12-May-2022].
- [30] N. Sánchez-Marroño, A. Alonso-Betanzos, and M. Tombilla-Sanromán, "Filter methods for feature selection. A comparative study."
- [31] H. Liu and L. Yu, "Toward Integrating Feature Selection Algorithms for Classification and Clustering," *IEEE Trans. Knowl. Data Eng.*, vol. 17, no. 4, pp. 491–502, Apr. 2005, doi: 10.1109/TKDE.2005.66.
- [32] M. Hall, "Correlation-based Feature Selection for Discrete and Numeric Class Machine Learning," in *Proc. 17th Int'l Conf. Machine Learning (ICML)*.
- [33] R. Kohavi and G. H. John, "Wrappers for feature subset selection," *Artif. Intell.*, vol. 97, no. 1–2, pp. 273–324, Dec. 1997, doi: 10.1016/S0004-3702(97)00043-X.
- [34] M. Dalponte, H. O. Ørka, T. Gobakken, D. Gianelle, and E. Næsset, "Tree species classification in boreal forests with hyperspectral data," *IEEE Trans. Geosci. Remote Sens.*, vol. 51, no. 5, pp. 2632–2645, 2013, doi: 10.1109/TGRS.2012.2216272.
- [35] L. Ma, M. M. Crawford, and J. Tian, "Local manifold learning-based k-nearest-neighbor for hyperspectral image classification," *IEEE Trans. Geosci. Remote Sens.*, vol. 48, no. 11, pp. 4099–4109, Nov. 2010, doi: 10.1109/TGRS.2010.2055876.
- [36] F. Melgani and L. Bruzzone, "Classification of hyperspectral remote sensing images with support vector machines," *IEEE Trans. Geosci. Remote Sens.*, vol. 42, no. 8, pp. 1778–1790, Aug. 2004, doi: 10.1109/TGRS.2004.831865.
- [37] K. Shang, X. Zhang, L. Zhang, and Y. Xie, "Evaluation of hyperspectral classification methods based on FISS data," *MIPPR 2011 Multispectral Image*

- Acquis. Process. Anal.*, vol. 8002, p. 80020L, Nov. 2011, doi: 10.1117/12.902908.
- [38] S. Shanmugam and P. SrinivasaPerumal, "Spectral matching approaches in hyperspectral image processing," *Int. J. Remote Sens.*, vol. 35, no. 24, pp. 8217–8251, Dec. 2014, doi: 10.1080/01431161.2014.980922.
- [39] L. Tan and M. Le Hou, "A study on the application of SAM classification algorithm in seal of calligraphy and painting based on hyperspectral technology," *4th Int. Work. Earth Obs. Remote Sens. Appl. EORSA 2016 - Proc.*, pp. 415–418, Aug. 2016, doi: 10.1109/EORSA.2016.7552841.
- [40] K. Kulkarni and P. A. Vijaya, "Experiment of multispectral images using spectral angle mapper algorithm for land cover classification," *Int. J. Innov. Technol. Explor. Eng.*, pp. 96–99, Mar. 2022, doi: 10.35940/IJITEE.F1018.0486S419.
- [41] R. H. Yuhas, A. F. Goetz, and J. W. Boardman, "Discrimination among semi-arid landscape endmembers using the Spectral Angle Mapper (SAM) algorithm," *JPL, Summ. Third Annu. JPL Airborne Geosci. Work. Vol. 1 AVIRIS Work.*, 1992.
- [42] Y. Guo, S. Han, Y. Li, C. Zhang, and Y. Bai, "K-Nearest Neighbor combined with guided filter for hyperspectral image classification," *Procedia Comput. Sci.*, vol. 129, pp. 159–165, Jan. 2018, doi: 10.1016/J.PROCS.2018.03.066.
- [43] H. M and S. M.N, "A Review on Evaluation Metrics for Data Classification Evaluations," *Int. J. Data Min. Knowl. Manag. Process*, vol. 5, no. 2, pp. 01–11, Mar. 2015, doi: 10.5121/IJDKP.2015.5201.
- [44] J. Lever, M. Krzywinski, and N. Altman, "Points of Significance: Classification evaluation," *Nat. Methods*, vol. 13, no. 8, pp. 603–604, Jul. 2016, doi: 10.1038/NMETH.3945.
- [45] M. Aron *et al.*, "Spectral imaging toolbox: Segmentation, hyperstack reconstruction, and batch processing of spectral images for the determination of cell and model membrane lipid order," *BMC Bioinformatics*, vol. 18, no. 1, pp. 1–8, May 2017, doi: 10.1186/S12859-017-1656-2/FIGURES/4.
- [46] I. Gerg, "MATLAB Hyperspectral Toolbox (<https://github.com/isaacgerg/matlabHyperspectralToolbox>), GitHub. Retrieved March 29, 2022." 2022.
- [47] E. Arzuaga-Cruz *et al.*, "A MATLAB toolbox for hyperspectral image analysis," *Int. Geosci. Remote Sens. Symp.*, vol. 7, pp. 4839–4842, 2004, doi: 10.1109/IGARSS.2004.1370246.
- [48] R. Farhoodi, V. Garousi, D. Pfahl, and J. Sillito, "Development of scientific software: A systematic mapping, a bibliometrics study, and a paper repository," *Int. J. Softw. Eng. Knowl. Eng.*, vol. 23, no. 4, pp. 463–506, May 2013, doi: 10.1142/S0218194013500137.

- [49] "MathWorks - Educators - MATLAB & Simulink." [Online]. Available: https://www.mathworks.com/academia/educators.html?s_tid=acmain_ep_gw_bod. [Accessed: 09-May-2022].
- [50] T. L. Saaty, "Exploring the interface between hierarchies, multiple objectives and fuzzy sets," *Fuzzy Sets Syst.*, vol. 1, no. 1, pp. 57–68, Jan. 1978, doi: 10.1016/0165-0114(78)90032-5.
- [51] L. Fang, S. Li, X. Kang, and J. A. Benediktsson, "Spectral-Spatial Classification of Hyperspectral Images with a Superpixel-Based Discriminative Sparse Model," *IEEE Trans. Geosci. Remote Sens.*, vol. 53, no. 8, pp. 4186–4201, Aug. 2015, doi: 10.1109/TGRS.2015.2392755.
- [52] R. H. Chan, K. K. Kan, M. Nikolova, and R. J. Plemmons, "A two-stage method for spectral-spatial classification of hyperspectral images," *J. Math. Imaging Vis.*, vol. 62, no. 6–7, pp. 790–807, Jul. 2020, doi: 10.1007/S10851-019-00925-9.
- [53] J. Nyman, "UPTec IT 18 003 Examensarbete 30 hp Pixel classification of hyperspectral images," 2018.
- [54] F. Cao, Z. Yang, J. Ren, M. Jiang, and W.-K. Ling, "Does Normalization Methods Play a Role for Hyperspectral Image Classification?," Oct. 2017, doi: 10.48550/arxiv.1710.02939.
- [55] H. Deborah, N. Richard, and J. Y. Hardeberg, "A Comprehensive Evaluation of Spectral Distance Functions and Metrics for Hyperspectral Image Processing," *IEEE J. Sel. Top. Appl. Earth Obs. Remote Sens.*, vol. 8, no. 6, pp. 3224–3234, Jun. 2015, doi: 10.1109/JSTARS.2015.2403257.
- [56] S. Addamani, "Spectral Angle Mapper Algorithm for Remote Sensing Image Classification," *IJISSET-International J. Innov. Sci. Eng. Technol.*, vol. 1, 2014.
- [57] A. Galal, H. Hasan, and I. F. Imam, "Learnable hyperspectral measures," *Egypt. Informatics J.*, vol. 13, no. 2, pp. 85–94, Jul. 2012, doi: 10.1016/J.EIJ.2012.04.004.
- [58] S. Alaliyat, "Video -based Fall Detection in Elderly's Houses," Gjøvik University College, 2008.
- [59] "Comparing GUIDE and App Designer - MATLAB & Simulink." [Online]. Available: <https://www.mathworks.com/products/matlab/app-designer/comparing-guide-and-app-designer.html>. [Accessed: 08-May-2022].
- [60] R. C. Gonzalez and R. E. Woods, *Digital Image Processing (3rd Edition)*. Pearson, 2007.
- [61] J. M. Amigo and S. Grassi, "Configuration of hyperspectral and multispectral imaging systems," *Data Handl. Sci. Technol.*, vol. 32, pp. 17–34, 2020, doi: 10.1016/B978-0-444-63977-6.00002-X.
- [62] M. E. Paoletti, J. M. Haut, J. Plaza, and A. Plaza, "Deep learning classifiers for

- hyperspectral imaging: A review," *ISPRS J. Photogramm. Remote Sens.*, vol. 158, pp. 279–317, Dec. 2019, doi: 10.1016/J.ISPRSJPRS.2019.09.006.
- [63] R. Madani, M. Tamre, and A. Tepljakov, "Development of a MATLAB GUI Application for Processing and Analysis of Hyperspectral Images ," in *Mekon 2021*, 2021.
- [64] "Specim IQ Technical Specifications - Specim." [Online]. Available: <https://www.specim.fi/iq/tech-specs/>. [Accessed: 08-May-2022].
- [65] "ENVI Header Files." [Online]. Available: <https://www.l3harrisgeospatial.com/docs/enviheaderfiles.html#Example>. [Accessed: 08-May-2022].
- [66] A. Zanchetta, "Remote Sensing Techniques for Change Detection Analysis in Arid and Semi-arid areas," Alan Turing Institute, 2017.
- [67] Y. W. Wang, N. P. Reder, S. Kang, A. K. Glaser, and J. T. C. Liu, "Multiplexed Optical Imaging of Tumor-Directed Nanoparticles: A Review of Imaging Systems and Approaches," *Nanotheranostics*, vol. 1, no. 4, p. 369, 2017, doi: 10.7150/NTNO.21136.
- [68] "Write hyperspectral data to ENVI file format - MATLAB enviwrite." [Online]. Available: <https://www.mathworks.com/help/images/ref/hypercube.enviwrite.html>. [Accessed: 10-May-2022].

APPENDICES

The appendices chapter of this thesis includes the following items:

- Specim IQ camera specifications
- Workflow of the Specim IQ camera
- ENVI Standard parameters for HS images
- Wavelength-Band Number mapping table
- Graphical material related to chapter 2
- Graphical material related to chapter 3
- The code
- The paper

APPENDIX 1 Specim IQ camera specifications

Table A1 Technical specifications of Specim IQ camera [64]

Parameter	Value
Spectral camera	VNIR 400-1000 nm (CMOS)
Viewfinder camera	5 Mpix
User interface SW	By Specim
Storage	SD card max 32 GB
Data Format	Specim Dataset with ENVI compatible data files
Battery	5200 mAh Li-Ion (Type 26650)
Operational time	Appx. 100 measurements with one SD card and battery
Display & keyboard	4.3 " touch screen + 13 physical buttons
Camera interface	USB Type-C, WiFi
Size	207 x 91 x 74 mm (depth with lens 125,5 mm)
Weight	1.3 kg
F/number	1.7
Wavelength band	400-1000 nm
Spectral resolution FWHM	7 nm
Spatial Sampling	512 pix
Spectral bands	204
Peak SNR	> 400:1
Object distance	150 – ∞ mm
FOV	31 x 31 deg
FOV at 1 m	0.55 x 0.55 m
Temperature, operational	+5°C – +40°C
Humidity, operational	95% non-condensing



Figure A1 Specim IQ camera

APPENDIX 2 Workflow of Specim IQ for imaging

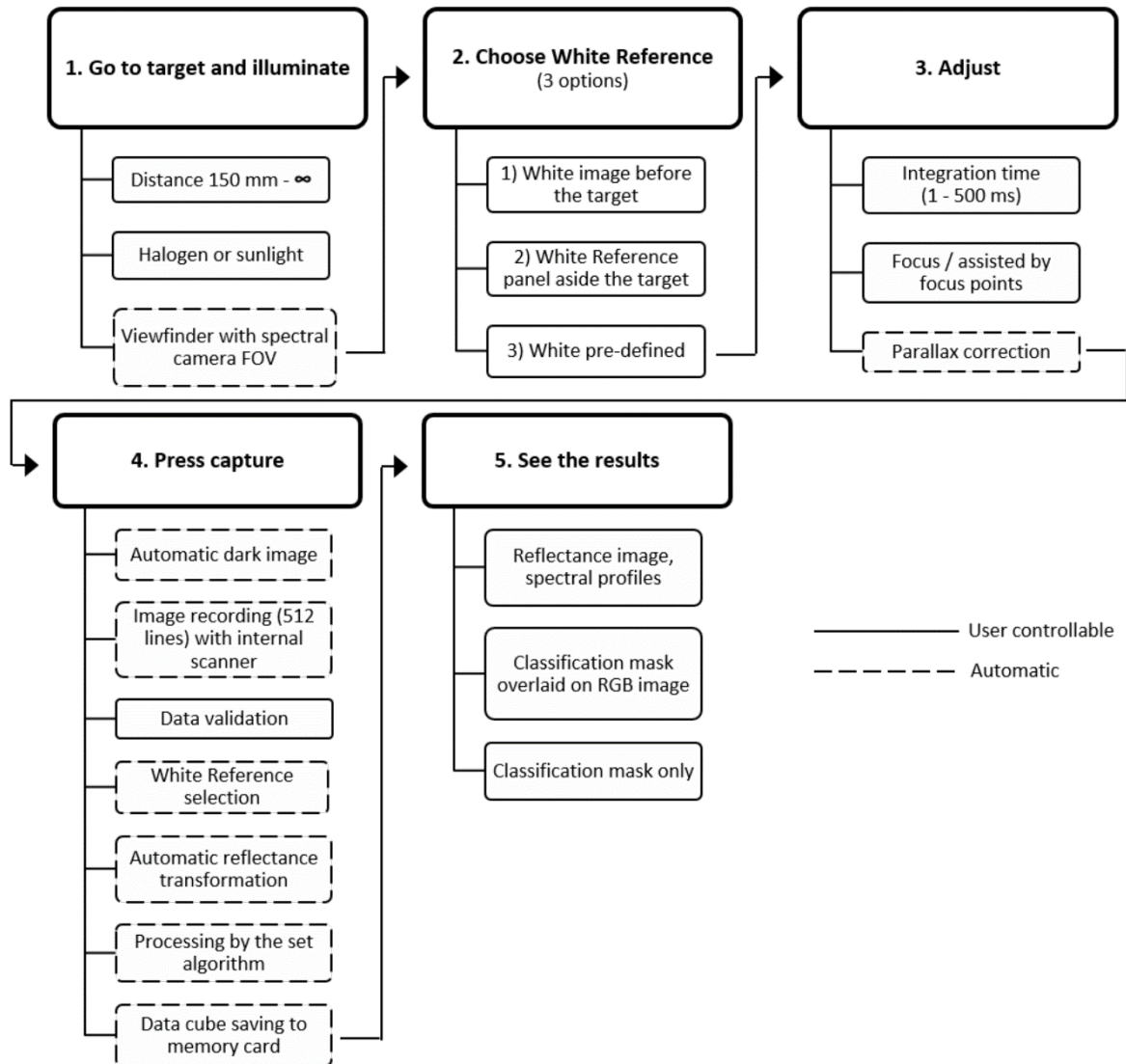


Figure A2 Detailed workflow of Specim IQ for the imaging procedure

APPENDIX 3 ENVI standard parameters for HS images

Table A2 ENVI parameter and its definition according to ENVI standard [65]

ENVI Header	Definition, Explanation
description	A character string describing the image or processing performed.
samples	Number of samples (pixels) per image line for each band.
lines	Number of lines per image for each band.
bands	Number of bands per image file.
header offset	Refers to the number of bytes of embedded header information present in the file (for example, 128 bytes for ERDAS 7.5 .lan files). These bytes are skipped when the ENVI file is read.
file type	Refers to specific ENVI-defined file types such as certain data formats and processing results.
data type	Parameter identifies the type of data representation:
	1 = 8-bit byte
	2 = 16-bit signed integer
	3 = 32-bit signed long integer
	4 = 32-bit floating point
	5 = 64-bit double precision floating point
	6 = 2x32-bit complex, real-imaginary pair of double precision
	9 = 2x64-bit double precision complex, real-imaginary pair of double precision (not supported in COMETOpticks)
	12 = 16-bit unsigned integer
	13 = 32-bit unsigned long integer
	14 = 64-bit unsigned integer (not supported in COMETOpticks)
15 = 64-bit unsigned long integer (not supported in COMETOpticks)	
interleave	Refers to whether the data are band sequential (BSQ), band interleaved by pixel (BIP), or band interleaved by line (BIL).
sensor type	Refers to specific instruments such as Landsat TM, SPOT, RadarSat, etc.
byte order	Describes the order of the bytes in integer, long integer, floating point, double precision, and complex data types.
	byte order=0 is Least Significant Byte First (LSF) data (DEC and MS-DOS systems) byte order=1 is Most Significant Byte First (MSF) data (all others - SUN, SGI, IBM, HP, DG).
x-start	Refer to the starting and ending sample and line if the image is a subset from a larger image.
y-start	
map info	Lists geographic coordinates information in the order projection name (UTM), magic pixel x value, magic pixel y value, magic pixel easting, magic pixel northing, x pixel size, y pixel size, Projection Zone, "North" or "South" for UTM only.

ENVI Header	Definition
projection info	Not supported by COMETOpticks.
default bands	If set, indicates which band numbers to automatically load into the Available Bands List's gray scale or R, G, and B text boxes every time the file is opened.
z plot range	Values indicating the default minimum and maximum values for Z plots.
z plot average	Values indicate the number of pixels in the X and Y directions to average for Z plots.
z plot titles	Allows entry of specific X and Y axis titles for Z plots.
pixel size	Indicates X and Y pixel size in meters for non-georeferenced files.
default stretch	Determines what type of stretch (% linear, linear range, Gaussian, equalize, square root) is used when the image is displayed.
band names	Allows entry of specific names for each band of an image.
wavelength	Lists the center wavelength values of each band in an image. Units should be the same as those used for the FWHM.
fwhm	Lists full-width-half-max values of each band in an image. Units should be the same as those used for wavelength.
bbl	Lists the bad band multiplier values of each band in an image, typically zero for bad bands and one for good bands.

APPENDIX 4 Wavelength-Band number mapping of Specim IQ

Table A3 List of the bands and their corresponding wavelengths in Specim IQ

Band No.	WL	Band No.	WL	Band No.	WL	Band No.	WL	Band No.	WL
1	397.32,	42	516.33,	83	637.08,	124	759.56,	165	883.79,
2	400.20,	43	519.25,	84	640.04,	125	762.57,	166	886.84,
3	403.09,	44	522.18,	85	643.01,	126	765.58,	167	889.90,
4	405.97,	45	525.10,	86	645.98,	127	768.60,	168	892.95,
5	408.85,	46	528.03,	87	648.95,	128	771.61,	169	896.01,
6	411.74,	47	530.96,	88	651.92,	129	774.62,	170	899.06,
7	414.63,	48	533.89,	89	654.89,	130	777.64,	171	902.12,
8	417.52,	49	536.82,	90	657.87,	131	780.65,	172	905.18,
9	420.40,	50	539.75,	91	660.84,	132	783.67,	173	908.24,
10	423.29,	51	542.68,	92	663.81,	133	786.68,	174	911.30,
11	426.19,	52	545.62,	93	666.79,	134	789.70,	175	914.36,
12	429.08,	53	548.55,	94	669.77,	135	792.72,	176	917.42,
13	431.97,	54	551.49,	95	672.75,	136	795.74,	177	920.48,
14	434.87,	55	554.43,	96	675.73,	137	798.77,	178	923.55,
15	437.76,	56	557.36,	97	678.71,	138	801.79,	179	926.61,
16	440.66,	57	560.30,	98	681.69,	139	804.81,	180	929.68,
17	443.56,	58	563.24,	99	684.67,	140	807.84,	181	932.74,
18	446.45,	59	566.18,	100	687.65,	141	810.86,	182	935.81,
19	449.35,	60	569.12,	101	690.64,	142	813.89,	183	938.88,
20	452.25,	61	572.07,	102	693.62,	143	816.92,	184	941.95,
21	455.16,	62	575.01,	103	696.61,	144	819.95,	185	945.02,
22	458.06,	63	577.96,	104	699.60,	145	822.98,	186	948.10,
23	460.96,	64	580.90,	105	702.58,	146	826.01,	187	951.17,
24	463.87,	65	583.85,	106	705.57,	147	829.04,	188	954.24,
25	466.77,	66	586.80,	107	708.57,	148	832.07,	189	957.32,
26	469.68,	67	589.75,	108	711.56,	149	835.11,	190	960.40,
27	472.59,	68	592.70,	109	714.55,	150	838.14,	191	963.47,
28	475.50,	69	595.65,	110	717.54,	151	841.18,	192	966.55,
29	478.41,	70	598.60,	111	720.54,	152	844.22,	193	969.63,
30	481.32,	71	601.55,	112	723.53,	153	847.25,	194	972.71,
31	484.23,	72	604.51,	113	726.53,	154	850.29,	195	975.79,
32	487.14,	73	607.46,	114	729.53,	155	853.33,	196	978.88,
33	490.06,	74	610.42,	115	732.53,	156	856.37,	197	981.96,
34	492.97,	75	613.38,	116	735.53,	157	859.42,	198	985.05,
35	495.89,	76	616.34,	117	738.53,	158	862.46,	199	988.13,
36	498.80,	77	619.30,	118	741.53,	159	865.50,	200	991.22,
37	501.72,	78	622.26,	119	744.53,	160	868.55,	201	994.31,
38	504.64,	79	625.22,	120	747.54,	161	871.60,	202	997.40,
39	507.56,	80	628.18,	121	750.54,	162	874.64,	203	1000.49,
40	510.48,	81	631.15,	122	753.55,	163	877.69,	204	1003.58
41	513.40,	82	634.11,	123	756.56,	164	880.74,		

APPENDIX 5 Graphical material related to Chapter 2

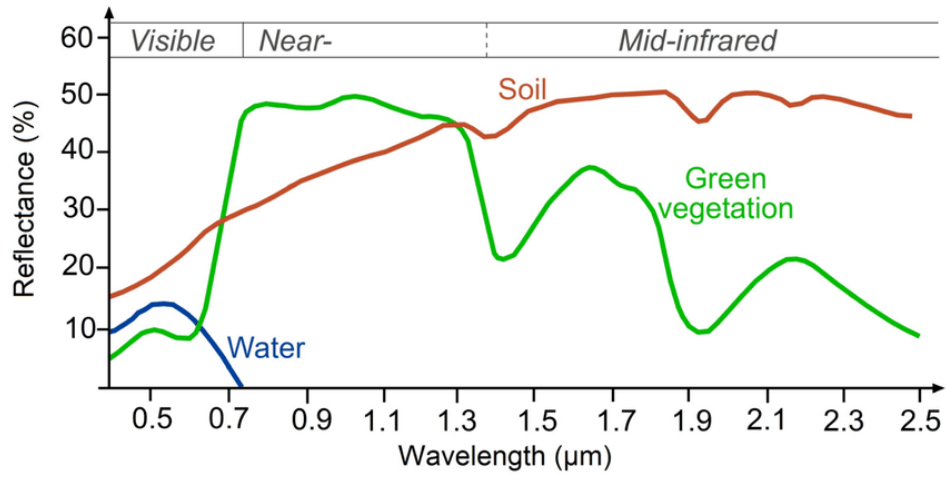


Figure A3 Spectral signature of different materials [66]

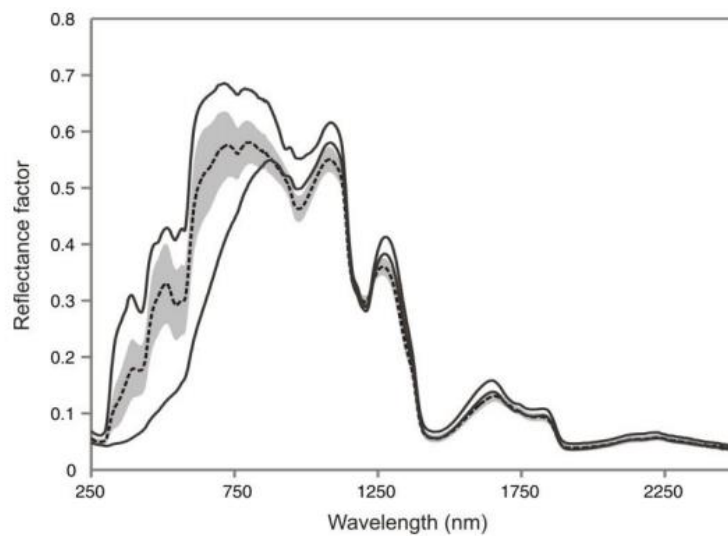


Figure A4 Image sample and spectral signatures of skins of 28 imaging subjects [26]

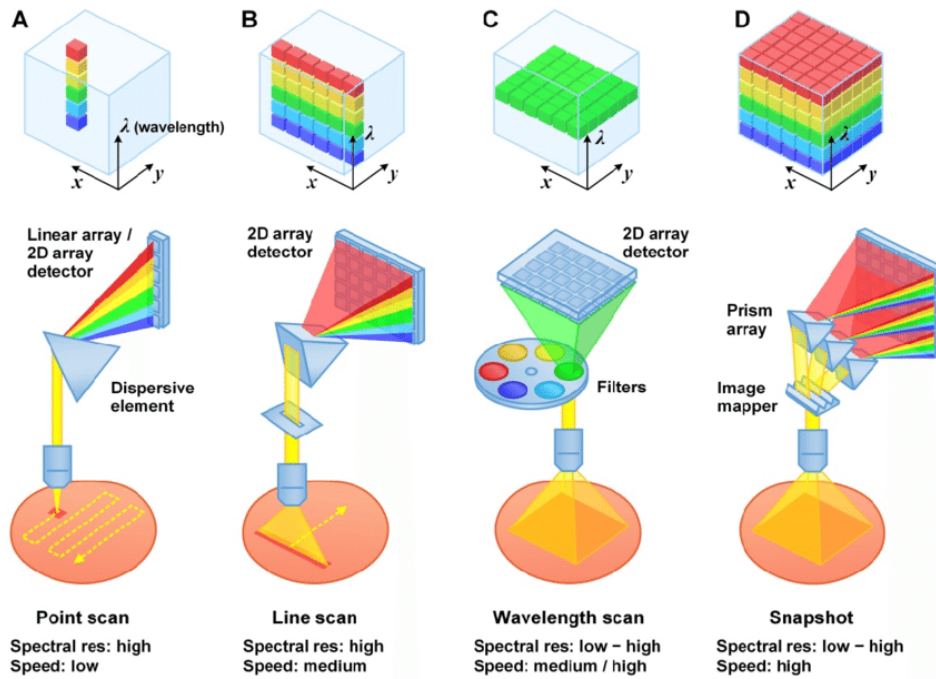


Figure A5 Different scanning techniques used in hyperspectral cameras [67]

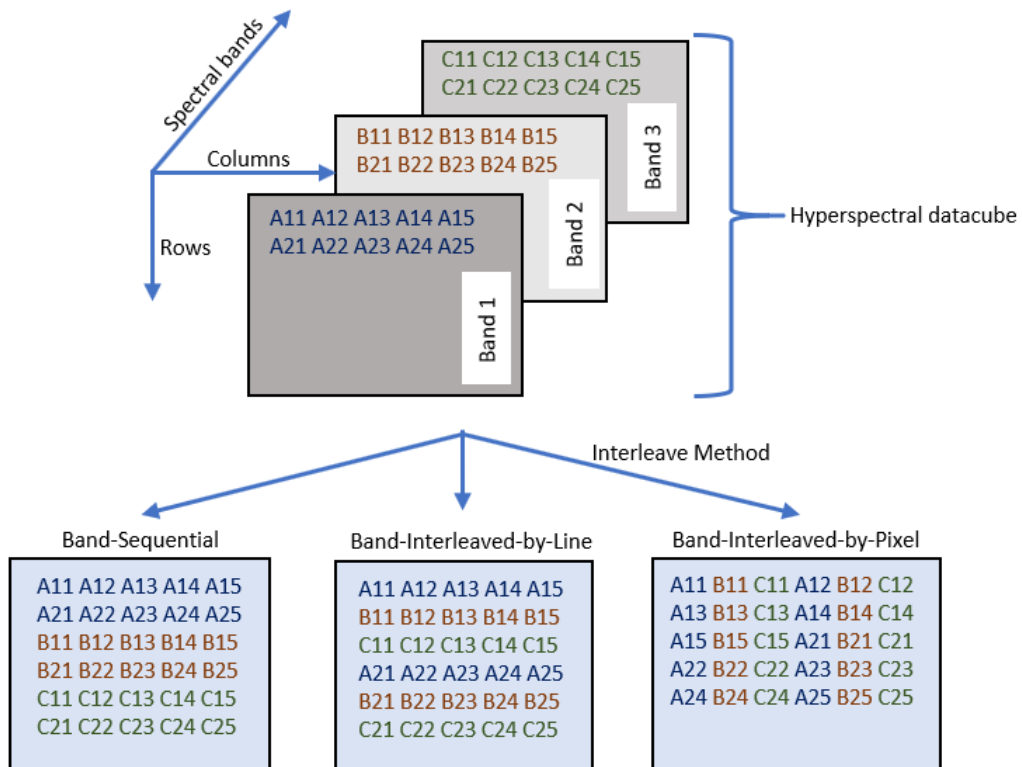


Figure A6 Three popular file structures of a hyperspectral image (BSQ, BIL, BIP) [68]

APPENDIX 6 Graphical material related to Chapter 3

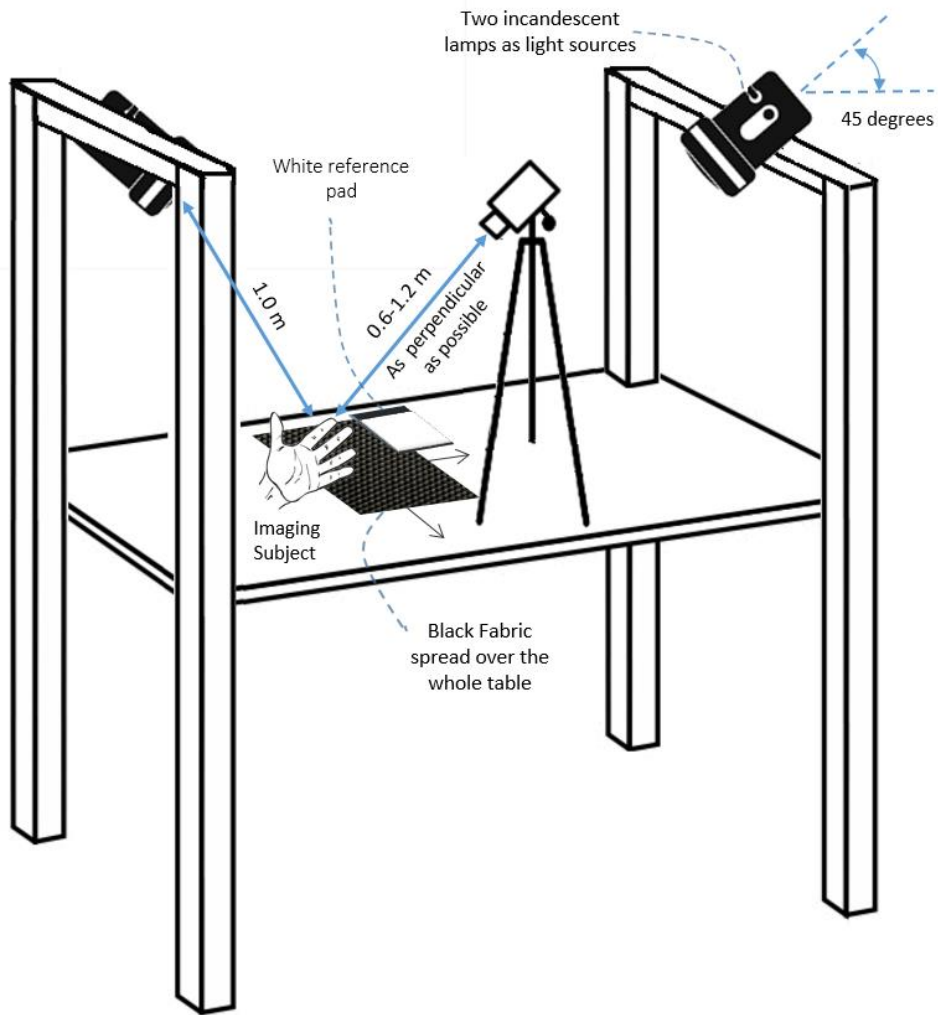


Figure A7 Imaging setup when the light source is incandescent light



Figure A8 Some skin samples collected in the dark room setup from different subjects and different parts of the body

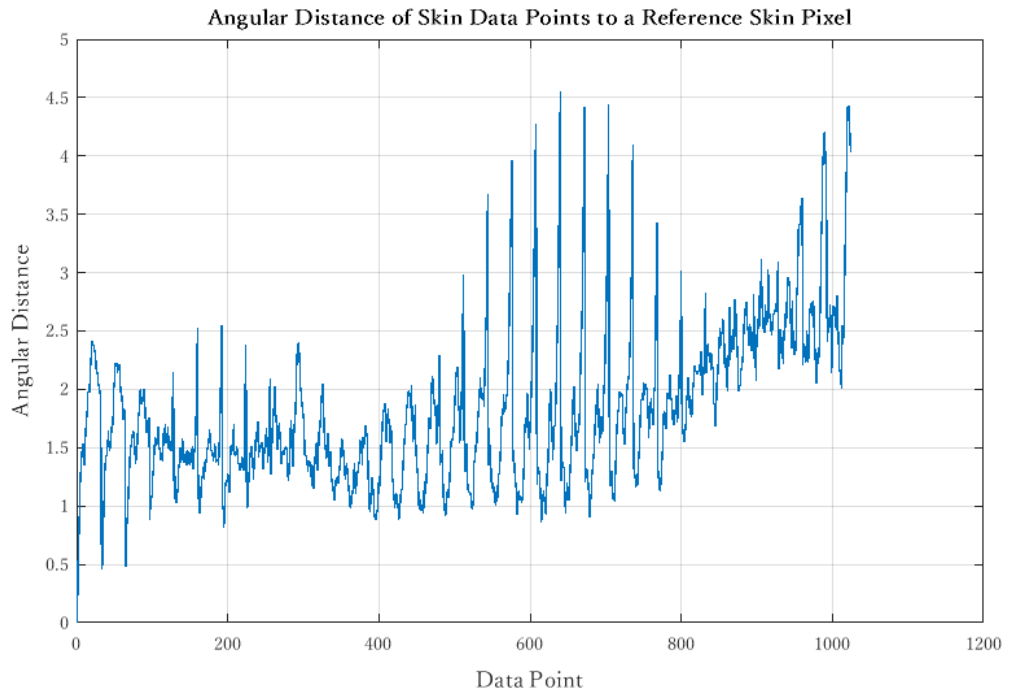


Figure A9 The range of the angular distances of the skin points to the reference point

APPENDIX 7 The Code

The developed code for the purpose of carrying out the research work is available at:

Madani, R (2022) Master [Source Code]. https://gitlab.cs.ttu.ee/ramada/thes_mas_1/

APPENDIX 8 The Paper

A paper was compiled on the subject of the GUI software tool presented in this thesis by the author of this thesis work, the main supervisor (Dr. Mart Tamre), and the co-supervisor (Dr. Aleksei Tepljakov):

Madani, R., Tamre, M., Tepljakov, A. (2021, June 25). Development of a MATLAB GUI Application for Processing and Analysis of Hyperspectral Images [Paper presentation] in Mekon 2021